Proton-Proton Interactions at 5.5 GeV/c

G. ALEXANDER, O. BENARY, G. CZAPEK,* B. HABER, N. KIDRON, B. REUTER, A. SHAPIRA, E. SIMOPOULOU,† AND G. YEKUTIELI

Nuclear Physics Department, Weizmann Institute of Science, Rehovoth, Israel

(Received 25 August 1966)

This report is based on about 10 500 pp collision events produced in the 81-cm Saclay hydrogen bubble chamber at CERN. Cross-section values for the different identified final states and resonances are given. The isobars N^*_{1238}, N^*_{1420}, N^*_{1518}, N^*_{1688}, N^*_{1920}, and N^*_{2360} were identified and their production cross-section values were found via a best-fit analysis of different invariant-mass histograms. About 70% of the isobars are connected with the quasi-two-body reactions $pp \to N^*N$ and $pp \to N^*N^*$. The reaction $pp \to nN^*_{1238}(p\pi^+)$ with a cross section of 3.25±0.16 mb was analyzed in terms of a peripheral absorption model, which was found to be in good agreement with the data. Various decay modes of the N^*_{1518} and N^*_{1688} isobars were observed and their branching ratios determined. The branching ratio of $n\pi^+$ to $p\pi^+\pi^-$ was found to be 0.77±0.45 for N^*_{1518} and 0.67±0.40 for N^*_{1688}. The branching ratio of $N^*_{1238}(p\pi^+)\pi^-$ to $p\pi^+\pi^-$ of N^*_{1688} was estimated to be 0.74±0.14. Pion production turned out to be mainly due to decay of isobars. Production of meson resonances turned out to be less important; the reaction $pp \to pp\omega^0 \to pp\pi^+\pi^-\pi^0$ was identified with a cross-section value of 0.11±0.02 mb. Finally, the production of neutral strange particles with a cross section of 0.45±0.04 mb is descussed. Strong formation of Y^*_{1385} is observed.

I. INTRODUCTION

IN this paper we present results of a comprehensive study of proton–proton interactions at 5.5 GeV/c. In particular we have investigated the contribution of the production of various isobars to the multipion final-state configurations in the pp collisions. Several reports on special aspects of this study, based on about a third of the number of events given here, have been published earlier,[1–5] and will be referred to whenever necessary. The results of this experiment are compared in the different sections with similar hydrogen-bubble-chamber work at various momenta.[6–10]

Section II is a description of the general experimental procedure, including exposure and event identification. Experimental results on the pp elastic scattering at 5.5 GeV/c are given in Sec. III. In Sec. IV the procedure which was used to fit various configurations of final-state particles and resonances to the invariant-mass distributions is described and evaluated. This procedure is then used in the later sections in which the different pp final states are analyzed. Finally in Sec. X we deal with the production of neutral strange particles in pp collisions.

II. EXPERIMENTAL PROCEDURE

The experiment was carried out with 30 000 pictures taken with the Saclay 81-cm hydrogen bubble chamber exposed to a secondary 5.5-GeV/c proton beam at CERN. Measurement on a sample of long incident proton tracks (longer than 50 cm) yielded an average momentum of 5.52±0.01 GeV/c. The contamination of the proton beam entering the bubble chamber was estimated by the δ-ray analysis method. A total contamination of 3.9% was found, of which about 1.5% was due to K^+ contamination and 2.4% to π^+, μ^+, and e^+ contamination.[11] The film was scanned twice for pp interactions in an inscribed fiducial volume, with an over-all efficiency of ~95%, yielding a total pp cross section of 41.6±1.4 mb. This value includes a correction of 1.35 mb due to loss of small-angle pp-elastic-scattering events described in Sec. III.

A random sample of about 10 500 pp collision events was measured and analyzed via the THRESH and GRIND programs. Ambiguous events were further resolved by ionization estimation. Cross-section values for the different final-state configurations are summarized in Table I together with results of earlier experiments at different momenta.

Among the two-prong events about 75% were identified uniquely to be one of the reactions (1), (2), and (3) described in Table I. Very few two-prong events yielded a good fit to reaction (1) as well as to reaction (2) or (3); but 53 events yielded good fit to both reactions (2) and (3). Part of the ambiguity between reactions (2) and (3) was resolved by angular-distribution considera-

* Also from the Physics Department, University of Bern, Bern, Switzerland.

† International Atomic Energy Fellow on leave from Nuclear Research Center "Democritos," Athens, Greece.

[1] G. Alexander, O. Benary, N. Kidron, A. Shapira, R. Yaari, and G. Yekutieli, Phys. Rev. Letters **13**, 355a (1964).

[2] G. Alexander, O. Benary, B. Reuter, A. Shapira, E. Simopoulou, and G. Yekutieli, Phys. Rev. Letters **15**, 207 (1965).

[3] G. Alexander, N. Kidron, B. Reuter, A. Shapira, and G. Yekutieli, Nuovo Cimento **39**, 384 (1965).

[4] G. Alexander, O. Benary, B. Haber, N. Kidron, A. Shapira, G. Yekutieli, and E. Gotsman, Nuovo Cimento **40A**, 839 (1965).

[5] G. Alexander, B. Haber, A. Shapira, G. Yekutieli, and E. Gotsman, Phys. Rev. **144**, 1122 (1966).

[6] G. A. Smith, H. Courant, E. C. Fowler, H. Kraybill, J. Sandweiss, and H. Taft, Phys. Rev. **123**, 2160 (1961).

[7] W. J. Fickinger, E. Pickup, D. K. Robinson, and E. O. Salant, Phys. Rev. **125**, 2082 (1962).

[8] D. V. Bugg, A. J. Oxley, J. A. Zoll, J. G. Rushbrooke, V. E. Barnes, J. B. Kinson, W. P. Dodd, G. A. Doran, and L. Riddiford, Phys. Rev. **133**, B1017 (1964).

[9] A. M. Eisner, E. L. Hart, R. I. Louttit, and T. W. Morris, Phys. Rev. **138**, B670 (1965).

[10] J. Kidd, L. Mandelli, V. Pelosi, S. Ratti, H. Sichirollo, L. Tallone, F. Conte, and G. Tomasini, Phys. Letters **16**, 75 (1965).

[11] B. Haber, M.Sc. thesis, Weizmann Institute of Science, 1964 (unpublished).

TABLE I. Summary of pp-final-state cross sections at 5.5 GeV/c compared with values obtained in earlier experiments at lower incident momenta.

	Final state	No. of events	$P=5.5$ GeV/c of this expt. (mb)	$P=3.68$ GeV/c of Ref. 9 (mb)	$P=2.81$ GeV/c of Ref. 8 (mb)	$P=2.23$ GeV/c of Ref. 7 (mb)	$P=1.66$ GeV/c of Ref. 6 (mb)
(1)	pp	2512	11.99 ±0.25	15.6 ±0.77	17.97±0.45	20.27±0.07	24.9 ±0.6
(2)	$pn\pi^+$	1682	8.03 ±0.19	11.65±0.66	15.02±0.41	17.57±0.60	18.4 ±0.7
(3)	$pp\pi^0$	581	2.77 ±0.11	2.95±0.31	3.60±0.21	4.06±0.27	3.7 ±0.3
	$2p+\geq 2$ neutrals	1645	7.85 ±0.20				
(4)	$pp\pi^+\pi^-$	1120	2.84 ±0.08	2.72±0.13	2.35±0.14	1.24±0.14	0.01±0.01
(5)	$pn\pi^+\pi^+\pi^-$	1127	2.85 ±0.08	1.17±0.09	0.38±0.04		0
(6)	$pp\pi^+\pi^-\pi^0$	729	1.84 ±0.07	0.75±0.07	0.20±0.03	0.02±0.02	0
	$4p+\geq 2$ neutrals	614	1.55 ±0.06				
(7)	$pp\pi^+\pi^+\pi^-\pi^-$	91	0.227±0.023				
(8)	$np\pi^+\pi^+\pi^+\pi^-\pi^-$	39	0.098±0.015				
(9)	$pp\pi^+\pi^+\pi^-\pi^-\pi^0$	36	0.088±0.014				
(10)	Neutral strange-particle production	156	0.45 ±0.04				

tions. The angular distributions of the two final-state nucleons in the unambiguous events shows a strong forward-backward correlation (Figs. 1 and 2). Using this correlation, some of the ambiguous events were identified by choosing the hypothesis in which the nucleons were definitely more forward-backward-peaked. A total of 1645 two-prong events did not fit any of the reactions (1), (2), and (3) and were therefore assumed to have more than one neutral particle in the final state.

In addition to the reactions (1), (2), and (3), we have also looked for the possible production of deuterium through the reaction $pp \rightarrow d\pi^+$. Most of the events which did fit the deuterium-production hypothesis also fitted other reactions, and hence it was practically impossible to evaluate a cross-section value for the reaction $pp \rightarrow d\pi^+$ in this experiment. Two events yielded a unique fit to the $pp \rightarrow d\pi^+$ reaction; however, one cannot rule out the possibility that these events may in fact be a reaction of the beam contamination such as $\pi^+p \rightarrow p\pi^+$. From the extrapolation of $\sigma(pp \rightarrow d\pi^+)$ data at lower incident proton momenta compiled by Cocconi *et al.*,[12] one expects a value of about 20 μb, which is equivalent in our experiment to approximately 4 events.

In this analysis of 3493 four-prong events, 2717 events yielded at least one good fit to the reactions (4–6) in Table I, 14 events were found unmeasurable, and the remaining 614 events did not yield any fit. Most of these remaining events were connected with a large missing mass and are presumably due to reactions with

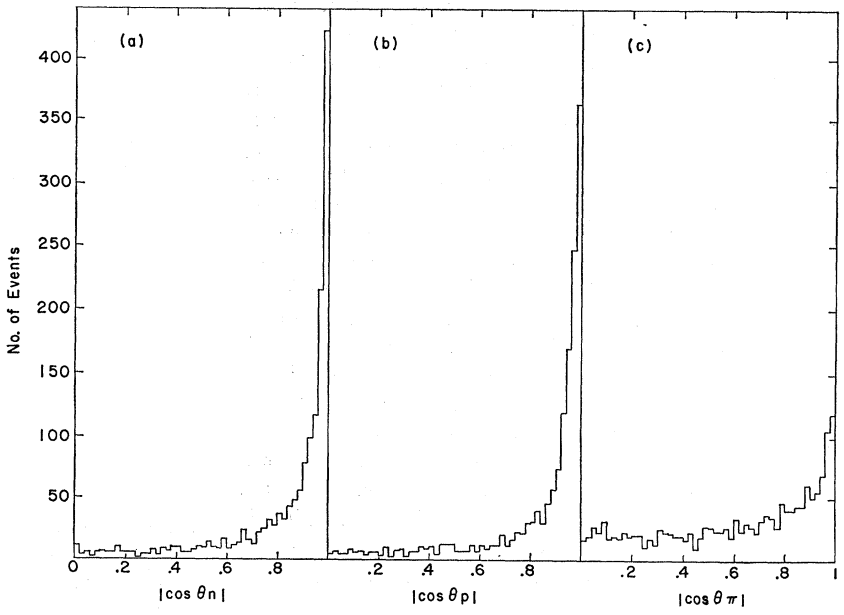

FIG. 1. Folded angular distribution of the $pn\pi^+$ final-state particles. (a) neutrons; (b) protons; (c) π^+ mesons.

[12] G. Cocconi, E. Lillethun, J. P. Scanlon, C. A. Stahlbrandt, C. C. Ting, J. Walters, and A. M. Wetherell, Phys. Letters 7, 222 (1963).

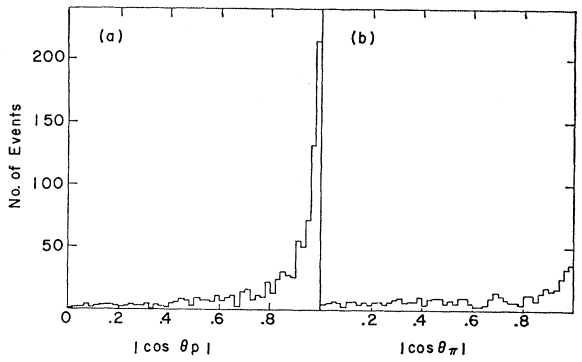

FIG. 2. Folded angular distribution of the $pp\pi^0$ final-state particles. (a) protons; (b) π^0 mesons.

more than one neutral particle in the final state. Most of the fitted events (~95%) were uniquely identified.

Six-prong events are rather rare at this incident proton momentum, and hence their study was extended to an additional 27 000 pictures taken in the same exposure. Altogether 355 six-prong events were found in the inscribed fiducial volume, out of which five events were found unmeasurable. In addition, 4 eight-prong events were found in the scan, out of which three yielded a good fit. The results of the 6-prong-event cross sections are given in Table I.

The production of neutral strange particles was also studied in 57 000 pictures. The film was specially scanned twice for events with neutral decays (V^0 events). A sample of 153 pp interactions associated with either Λ or K_1^0 decay events was found in the inscribed fiducial volume with an over-all efficiency of 99%. Among these, 112 events yielded a unique fit to the strange-particle-production hypothesis, 18 events yielded two good fits, and 23 events failed to yield any good fit. Of the unfitted events, 14 were associated with large missing mass and were assumed to have more than one neutral particle in the final state. The remaining 9 events are attributed to measurement difficulties, contamination events, or V^0 decay too near to the apex to be measurable. Another three Λ decay events in which the Λ interacted with a proton in the chamber were also used for the cross-section evaluation. A cutoff of 3 mm in the projected plane was imposed on all single-V^0 events, and each accepted event was weighted accordingly. In addition, to each event there was also assigned a weight for unobservable decays and scanning losses. The weights were calculated using the branching ratios given by Rosenfeld *et al.*[13] and assuming an equal production rate for K_1^0 and K_2^0. The over-all cross section for V^0 production in this experiment is given in Table I; detailed cross section values for the different V^0 final-state configurations are discussed in Sec. X.

[13] A. H. Rosenfeld, A. Barbaro-Galtieri, W. H. Barkas, P. L. Bastien, J. Kirz, and M. Roos, Rev. Mod. Phys. 37, 633 (1965).

III. ELASTIC SCATTERING

The experimental differential cross-section distribution folded around 90° is shown in Fig. 3 as a function of the invariant momentum transfer squared, t, of the unambiguous events. Also shown in this figure is the "optical point" $(d\sigma/dt)_{t=0}=\sigma_{\text{tot}}^2/16\pi$ calculated from the total pp cross section of 41.6±1.4 mb measured in this experiment. As can be seen from Fig. 3 there is a definite loss of small-angle scattering events below a momentum transfer of $|t|<0.03$ $(\text{GeV}/c)^2$ which was taken as the lower experimental cutoff for the following analysis. The data were analyzed in terms of two spin-independent expressions for the differential cross section of the type $d\sigma/dt=\exp(a+bt)$ and $d\sigma/dt=\exp(A+Bt+Ct^2)$, omitting the Coulomb-scattering contribution, which is negligible in the region $t>0.03$ $(\text{GeV}/c)^2$. The best values for the parameters a, b, A, B, and C are given in Table II. They were obtained from a fit to the data inside the region of $0.03\leqslant|t|\leqslant0.75$ $(\text{GeV}/c)^2$. These values varied only slightly with a change in the momentum-transfer region used for the fit. The value of the parameter b may be associated with an interaction radius r of an opaque diffraction sphere with a sharp boundary through the relation $r=2(-b)^{1/2}$. The value obtained for r is also given in Table II. The present results are compared in Table II with results given by Harting *et al.* at higher incident proton momenta of 8.5, 12.4, and 18.4 GeV/c.[14]

Recent data on pp elastic scattering have shown that the real part of the forward scattering amplitude Re $f(0)$ is not zero. The value of $\alpha=\text{Re}\,f(0)/\text{Im}\,f(0)$ has

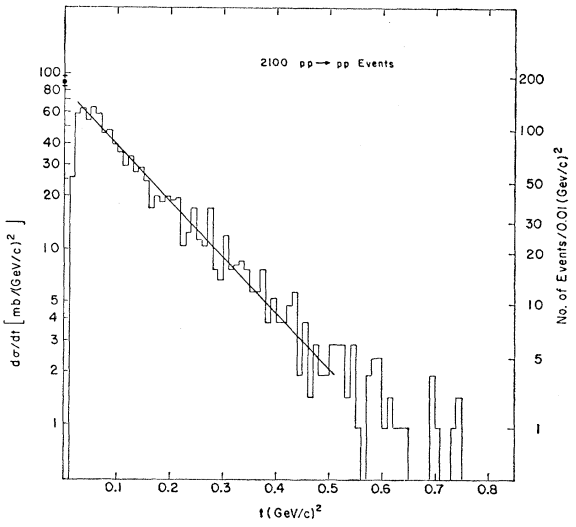

FIG. 3. Differential cross section of the reaction $pp\rightarrow pp$. Solid line represents best fit of the data to the expression $d\sigma/dt=\exp(A+Bt+Ct^2)$.

[14] D. Harting, P. Blackall, B. Elsner, A. C. Helmholtz, W. C. Middelkoop, B. Powell, B. Zacharov, P. Zanella, P. Dalpiaz, M. N. Focacci, S. Focardi, G. Giacomelli, L. Monari, J. A. Beaney, R. A. Donald, P. Mason, L. W. Jones, and D. O. Caldwell, Nuovo Cimento 38, 60 (1965).

TABLE II. Best-fit values of the elastic pp collisions to the expressions $d\sigma/dt=\exp(a+bt)$ and $d\sigma/dt=\exp(A+Bt+Ct^2)$. The last row gives the "optical point". The results of the present experiment are compared with results of Harting *et al.* (Ref. 14) at 8.5, 12.4, and 18.4 GeV/c.

Incident p momentum (GeV/c)	5.5	8.5	12.4	18.4
Reference	Present experiment	Harting *et al.* Ref. 14	Harting *et al.* Ref. 14	Harting *et al.* Ref. 14
$\|t\|$ Range (GeV/c)^2	0.03–0.75	0.13–0.50	0.13–0.50	0.13–0.50
a	4.39 ±0.04	4.198±0.028	4.150±0.033	4.178± 0.080
b [(GeV/c)$^{-2}$]	−7.17 ±0.18	−7.75 ±0.11	−8.19 ±0.13	−8.58 ± 0.25
r (fermi)	1.056±0.014	1.099±0.008	1.129±0.009	1.156± 0.016
$\|t\|$ Range (GeV/c)^2	0.03–0.75	0.13–0.95	0.13–0.95	0.13–0.95
A	4.45 ±0.05	4.241±0.044	4.259±0.053	4.391±0.131
B [(GeV/c)$^{-2}$]	−7.96 ±0.41	−8.16 ±0.28	−9.05 ±0.34	−9.79 ± 0.63
C [(GeV/c)$^{-4}$]	1.50 ±0.75	0.84 ±0.36	1.41 ±0.44	1.53 ±0.69
e^A [mb/(GeV/c)^2]	85.9 ±4.0	69.5 ±3.1	70.7 ±3.8	80.7 ±10.6
$\sigma_{\text{tot}}^2/16\pi$ [mb/(GeV/c)^2]	88.9 ±5.4	83.7 ±4.1	79.7 ±4.0	79.7 ± 4.0

also been estimated from dispersion relations[15,16] and was found to be in good agreement with the experimental data.[17] From these dispersion-relation calculations it is expected that α will be equal to about -0.3 at an incident proton momentum of 5.5 GeV/c, corresponding to an increase in $(d\sigma/dt)_{t=0}$ of about 10% above the "optical point." In this experiment no meaningful value of α could be derived, because of the limited statistics, the loss of small-angle scattering events, and the error in the total pp cross section. In fact the value of $(d\sigma/dt)_{t=0}$ derived from the fit to the expression $d\sigma/dt=\exp(A+Bt+Ct^2)$ is lower than the "optical point" by about one standard deviation. The same situation obtains in the fit to the data of Harting *et al.*[14] at 8.5 and 12.4 GeV/c (see Table II). The total elastic-scattering cross section given in Table I has been obtained by integrating the differential cross section and extrapolating it to a point 10% above the "optical point.

IV. METHOD FOR RESONANCE CROSS-SECTION EVALUATION

The major part, about 75%, of the total-pp cross section at 5.5 GeV/c is due to pion-producing reactions. The pions are produced directly or through intermediate states of baryonic or mesonic resonances. In the following chapters the different final-state configurations listed in Table I are studied. In this study we try to identify the different resonance channels that participate in each final-state configuration and to evaluate their partial cross sections. The main tool in this research program is the best-fit analysis to the various observed invariant-mass histograms. The relative rates of the different resonance channels are found in each case by a maximum-likelihood fit between, on the one hand, the observed invariant mass histogram, and on the other hand, a linear combination of phase-space and corresponding mass distributions of the resonance channels.

In this analysis only well-established resonances were taken into account. The possibility of new resonances was considered only when the data could not have been otherwise explained.

The validity of such a method is mainly based on the following assumptions:

(a) The reactions leading to the final-state particles can be described in terms of independent partial channels; and the total final-state cross section is the sum of the partial-channel cross sections.

(b) Interference effects between the various channels can be neglected.

The invariant-mass distributions of ordinary phase space and resonance channels were evaluated after Pinski.[18] This method was also used to calculate mass distributions of simple configurations with a cutoff at a small invariant momentum transfer Δ^2. More complicated invariant-mass distributions were calculated, and in particular a study of peripheral effects was made, via a Monte-Carlo-type calculation using the program RANDSTAR.[19] In forming the invariant-mass distributions the ambiguity of the two identical particles in a final state like $p_1p_2\pi^+\pi^-$ was treated in two ways: (a) Both combinations including the identical particles were taken. In this method the proper invariant-mass distributions f of the two protons were evaluated; for example: $f=f_1(M(p_1\pi^+))+f_2(M(p_2\pi^+))$. (b) Only one combination, with the minimum momentum transfer Δ^2, was chosen for the invariant-mass histograms. This was achieved in two steps. In the first, each (say) $p\pi^+$ combination, was assigned a momentum transfer $\Delta^2(p\pi^+)$ which was defined as the minimum momentum transfer of the combination to the incident and target protons: $\Delta^2(p\pi^+)=\min[\Delta_i^2(p\pi^+);\ \Delta_t^2(p\pi^+)]$. This step is equivalent to a fold in the angular distribution

[15] P. Söding, Phys. Letters 8, 285 (1964).
[16] I. I. Levintov and G. M. Adelson-Velsky, Phys. Letters 13, 185 (1964).
[17] S. J. Lindenbaum, in *Proceedings of the Oxford International Conference on Elementary Particles, 1965* (Rutherford High Energy Laboratory, Harwell, England, 1966), p. 93.
[18] G. Pinski, Nuovo Cimento 24, 719 (1962).
[19] G. Yekutieli (unpublished).

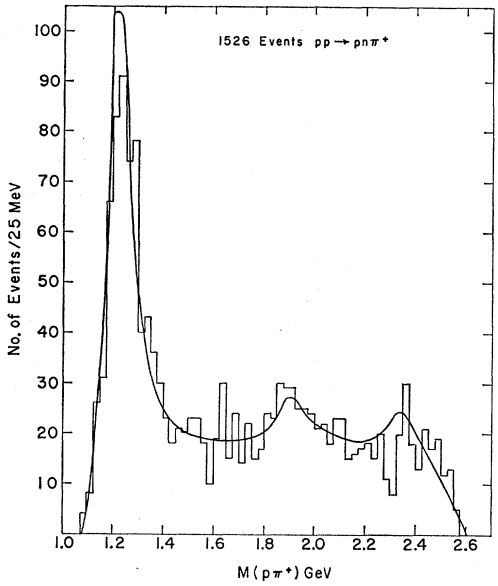

FIG. 4. Invariant-mass distribution of $p\pi^+$ in the reaction $pp \rightarrow pn\pi^+$.

through 90°. The second step was to choose that $p\pi^+$ combination with the minimal value of Δ^2. This choice of double-minimum delta (DMD) may be justified only for peripheral reactions.

The mixture of channels for any particular invariant mass histogram was found by maximizing the likelihood function

$$L=\prod_{i=1}^{m} \frac{f(i)^{n_i} \exp[-f(i)]}{n_i!},$$

where $f(i)$ and n_i are the expected and observed numbers of events in the ith bin of the mass plot. The error of the best set of channels rates $a_1, a_2, \cdots a_k$ was found by varying the likelihood function $L(a_1,a_2,\cdots a_k)$ by one standard deviation, that is $L(a_j \pm \Delta a_j)=L(a_j)/\sqrt{e}$. In this estimate of the error we have varied together with a_j only the rate of the most competing channel, leaving all other rates fixed. It was found that in simple cases the error Δa_j thus calculated for resonance production was in fact very near to the statistical error $1/\sqrt{N}$, where N was the number of events in the resonance peak.

The partial-cross-section values obtained in this way (Tables III to VI) thus represent the relative percentage of the different channels for which their combined mass distribution best fitted the data; the reliability of these values is subject to the assumptions discussed earlier and to the validity of the calculated invariant mass distributions. The errors given in the tables are evaluated from the fit only.

V. $pp \rightarrow NN\pi$ REACTIONS

The reactions $pp \rightarrow pn\pi^+$ and $pp \rightarrow pp\pi^0$ were analyzed in terms of various $N^*_{1/2}$ and $N_{3/2}$* productions in the reaction $pp \rightarrow N^*N$ with a subsequent $N^* \rightarrow N\pi$ decay. In Figs. 4 and 5 are plotted the invariant-mass distributions of the $p\pi^+$ and $n\pi^+$ combinations of the uniquely identified events, and in Fig. 6 the scatter diagram of $M^2(p\pi^+)$ versus $M^2(n\pi^+)$. In the $M(p\pi^+)$ there is a strong formation of $N^*_{1238}(p\pi^+)$ and weaker formation of $N^*_{1920}(p\pi^+)$. There is also evidence for

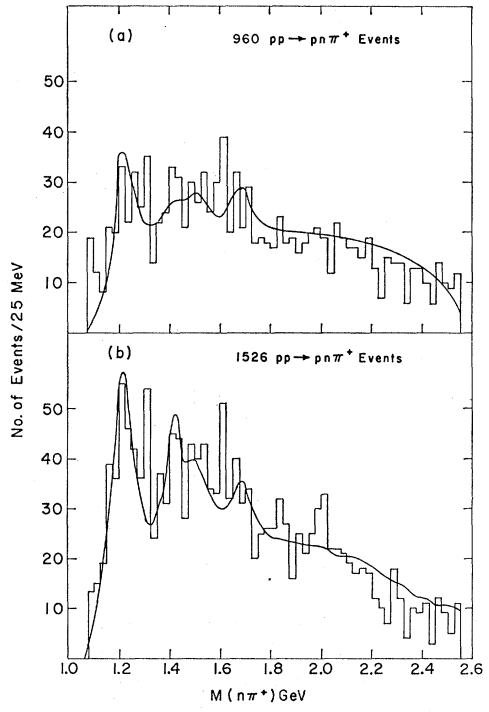

FIG. 5. Invariant-mass distributions of $n\pi^+$ configuration in the reaction $pp \rightarrow pn\pi^+$. (a) excluding events with $M(p\pi^+)$ in the $N^*_{1238}(p\pi^+)$ region; (b) all events.

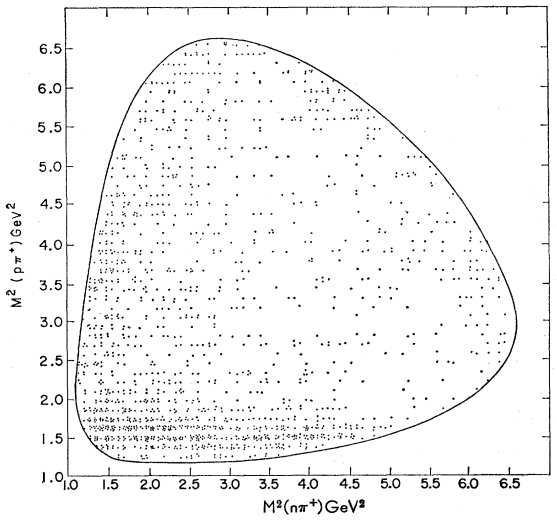

FIG. 6. Dalitz plot of $M^2(p\pi^+)$ versus $M^2(n\pi^+)$ in the $pp \rightarrow pn\pi^+$ reaction.

the formation of $N^*_{2360}(p\pi^+)$, which is, however, less reliable, particularly since events in this region have a somewhat higher probability of remaining ambiguous after the fit and the ionization estimation.

The isobar production cross section has been evaluated through a fit of the invariant-mass histograms to a linear combination of $NN\pi$ phase space and to N^*N with subsequent $N^* \rightarrow N\pi$ distributions. The latter distribution used was of the form[20]:

$$f(M_{12}) \propto \frac{\Gamma(M_{12})Q_N}{(M_{N^*}{}^2 - M_{12}{}^2)^2 + M_{N^*}{}^2\Gamma^2(M_{12})};$$

$$\Gamma(M_{12}) \approx \Gamma_0(q/q_0)^{2l+1},$$

where M_{N^*} is the mass of the resonance; M_{12} is the invariant mass of the $N\pi$ configuration; Γ_0 is the width of the resonance; q is the momentum of the pion in the M_{12} center-of-mass system; q_0 is the value of q at $M_{12}=M_{N^*}$, l is the orbital angular momentum of the N^* resonance; and Q_N is the momentum of the spectator nucleon in the pp center-of-mass system.

The result of the best fit to the $M(p\pi^+)$ is shown in Fig. 4 and in Table III. The same fitting procedure was adopted for the $M(n\pi^+)$ histogram, where the data were fitted with a linear combination of phase space, N^*_{1238}, N^*_{1420}, N^*_{1518}, and N^*_{1688} distributions. The best fit is shown in Fig. 5(a) for the $M(n\pi^+)$ histogram, where all events with $M(p\pi^+)$ in the $N^*_{1238}(p\pi^+)$ region where removed. In Fig. 5(b) the fit to $M(n\pi^+)$ using all events is shown. The first method is less affected by our knowledge of the influence of $N^*_{1238}(p\pi^+)$ on the $M(n\pi^+)$ distribution. Both methods yielded approximately the same results, apart from the case of $N^*_{1238}(n\pi^+)$ production, where the first method yielded a value for the cross section of 0.75±0.08 mb and the second 1.48±0.16 mb. The results of the best fit are shown in Table III; the value given for $pp \rightarrow N^*_{1238}(n\pi^+)p$ is the one obtained from the first method.

TABLE III. Partial cross sections of channels contributing to the $np\pi^+$ and $pp\pi^\circ$ final states, compared with isospin predictions. Errors quoted are from best-fit procedure only.

	Channel	σ(mb)	Isospin branching-ratio predictions
A	$N^{*++}_{1238}(p\pi^+)n$	3.25±0.16	9/12
B	$N^{*+}_{1238}(n\pi^+)p$	0.75±0.08	1/12
C	$N^{*+}_{1238}(p\pi^0)p$	0.72±0.05	2/12
D	$N^{*++}_{1920}(p\pi^+)n$	0.32±0.16	9/12
E	$N^{*+}_{1920}(n\pi^+)p$	0	1/12
F	$N^{*+}_{1920}(p\pi^0)p$	0	2/12
G	$N^{*++}_{2360}(p\pi^+)n$	0.20±0.08	9/12
H	$N^{*+}_{2360}(n\pi^+)p$	0	1/12
I	$N^{*+}_{2360}(p\pi^0)p$	0	2/12
J	$N^{*+}_{1420}(n\pi^+)p$	0.80±0.16	2/3
K	$N^{*+}_{1420}(p\pi^0)p$	0.36±0.06	1/3
L	$N^{*+}_{1518}(n\pi^+)p$	0.44±0.20	2/3
M	$N^{*+}_{1518}(p\pi^0)p$	0±0.04	1/3
N	$N^{*+}_{1688}(n\pi^+)p$	0.32±0.16	2/3
O	$N^{*+}_{1688}(p\pi^0)p$	0.22±0.06	1/3

[20] J. D. Jackson, Nuovo Cimento 34, 1644 (1964).

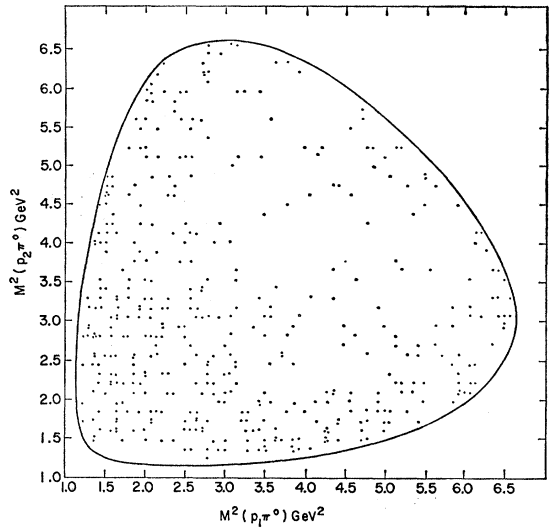

FIG. 7. Dalitz plot of $M^2(p_2\pi^0)$ versus $M^2(p_1\pi^0)$ in the $pp \rightarrow pp\pi^0$ reaction.

The Dalitz plot for the final state in the reaction $pp \rightarrow pp\pi^0$ is shown in Fig. 7, and in Fig. 8 the invariant-mass distribution $M(p\pi^0)$ is presented for both $p\pi^0$ combinations of each event. There is some indication for the production of $N^*_{1238}(p\pi^0)$, $N^*_{1420}(p\pi^0)$, and $N^*_{1688}(p\pi^0)$. The best fit to the data is shown in Fig. 8 and the corresponding cross section values are given in Table III. Finally the values for the isobar production cross sections are compared with predicted branching ratios obtained from isospin considerations (Table III).

The production angular distribution of $M(p\pi^+)$ in the $N^*_{1238}(p\pi^+)$ region of 1.18–1.30 GeV is shown in Fig. 9. In the same figure the expected $pp \rightarrow N^*_{1238}n$ pro-

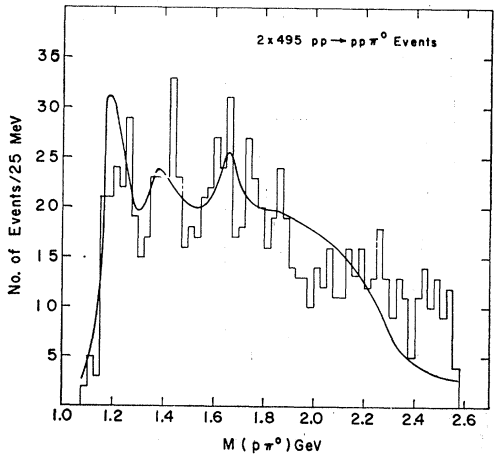

FIG. 8. Invariant-mass distribution of $p\pi^0$ in the $pp \rightarrow pp\pi^0$ reaction.

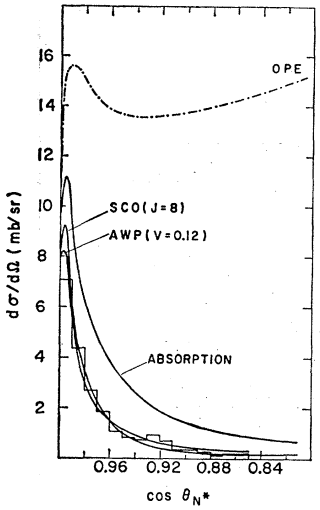

FIG. 9. Differential cross section of the $pp \to nN^*_{1238}$ reaction. The curves correspond to calculated cross sections with the unmodified OPE model and with modified OPE models using different forms of absorption corrections (see text).

duction differential cross section $d\sigma/d\Omega$ is shown for the simple one-pion-exchange (OPE) model (dashed line), and for the OPE model taking into account effects arising from competing channels (solid lines) in the absorption models. The absorption modifications to the OPE model used in this work are described in detail in an earlier paper.[5] In Fig. 9 the solid line marked "absorption" is obtained by taking the absorption factor from the elastic scattering $pp \to pp$ information obtained in this work and assuming that the same $d\sigma/d\Omega$ behavior describes the $N^*_{1238}n$ elastic scattering. In the method of absorption with free parameter (AWP), the elastic scattering of $N^*_{1238}n$ was taken as a free parameter which was fitted to the data. The best fit obtained was $\nu=0.12$, where ν is defined through the expression $d\sigma/dt=(\sigma_{\text{tot}}^2/16\pi)\exp[-(t/2)\nu^2]$. The last method applied to the data was the sharp-cutoff (SCO) method, where only partial waves of $J<J_c$ contribute to the absorption channels. The result for the best value $J_c=8$ is shown in Fig. 9.

In Fig. 10 the decay distributions of the $p\pi^+$ combination inside (a,b) and outside (c,d) the N^*_{1238} invariant-mass region are shown. The angles θ and φ are described in a reference frame in which the z axis is parallel to the direction of the incoming proton, the y axis is perpendicular to the $p\pi^+$ production plane, and the x axis is perpendicular to the y–z plane. In this frame of reference the angular distribution of the N^*_{1238} decay proton is given by[21]

$$W(\cos\theta,\varphi)=(3/4\pi)\{\rho_{3,3}\sin^2\theta+\rho_{1,1}(\tfrac{1}{3}+\cos^2\theta)-\tfrac{2}{3}\sqrt{3}(\mathrm{Re}\rho_{3,-1}\sin^2\theta\cos2\varphi+\mathrm{Re}\rho_{3,1}\sin2\theta\cos\varphi)\},$$

where $\rho_{m,m'}$ are the density-matrix elements. The values of $\rho_{3,3}$, $\mathrm{Re}\rho_{3,-1}$, and $\mathrm{Re}\rho_{3,1}$ for the simple OPE model, OPE with absorption, OPE with AWP, and SCO, as functions of $\cos\theta$, are shown in Fig. 11. In the same figure are also shown the parameters ρ as obtained from the data. The full circles are calculated from the total sample, the hollow circles from data at different $\cos\theta$ regions.

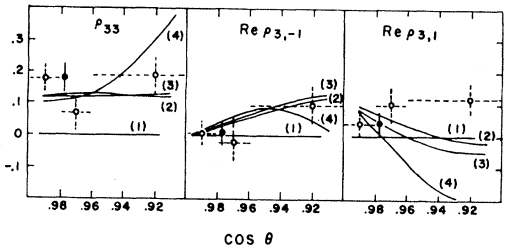

FIG. 11. Experimental values of the parameter ρ for the total sample (filled circles) and for different $\cos\theta$ intervals (open circles). The curves correspond to calculated ρ values using the different OPE models. (1—OPE; 2—ABS; 3—AWP; 4—SCO.)

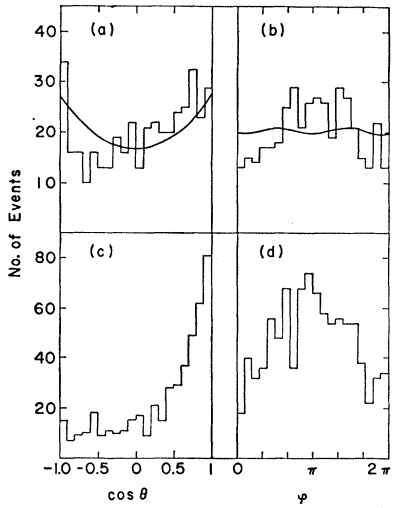

FIG. 10. The distribution of $\cos\theta$ and φ, where θ and φ are the angles of the decay proton in the N^*_{1238} c.m. system. (a) and (b) correspond to events with 1170 MeV$\leq M(p\pi^+)\leq$1300 MeV; (c) and (d) correspond to events with $1300\leq M(p\pi^+)\leq 1800$ MeV. Solid lines represent best fit to the data.

Several experiments on the production of isobars in the reaction $pp \to N^*_{1238}p$ have been reported at different energies using counter techniques.[22–24] Anderson *et al.*[24] have studied the reaction $pp \to N^*_{1238}p$ at 6 GeV/c, that is 0.5 GeV/c higher than the present experiment. The N^*_{1238} was studied in the momentum-transfer region $0.01\leq\Delta^2\leq 0.11$ (GeV/c)^2 and the differential cross section was fitted with the expression $d\sigma/dt=A\exp(-b|t|)$. The best values obtained in the

[21] K. Gottfried and J. D. Jackson, Nouvo Cimento **33**, 309 (1964).

[22] G. Cocconi, E. Lillethun, J. P. Scanlon, C. A. Stahlbrandt, C. C. Ting, J. Walters, and A. M. Wetherell, Phys. Letters **8**, 134 (1964).

[23] C. M. Ankenbrandt, A. R. Clide, B. Cork, D. Keefe, L. T. Kerth, W. M. Layson, and W. A. Wenzel, Nuovo Cimento **35**, 1052 (1965).

[24] E. W. Anderson, E. J. Bleser, G. B. Collins, T. Fujii, J. Menes, F. Turkot, R. A. Carrigan, Jr., R. M. Edelstein, N. C. Hien, T. J. McMahon, and I. Nadelhaft, Phys. Rev. Letters **16**, 855 (1966).

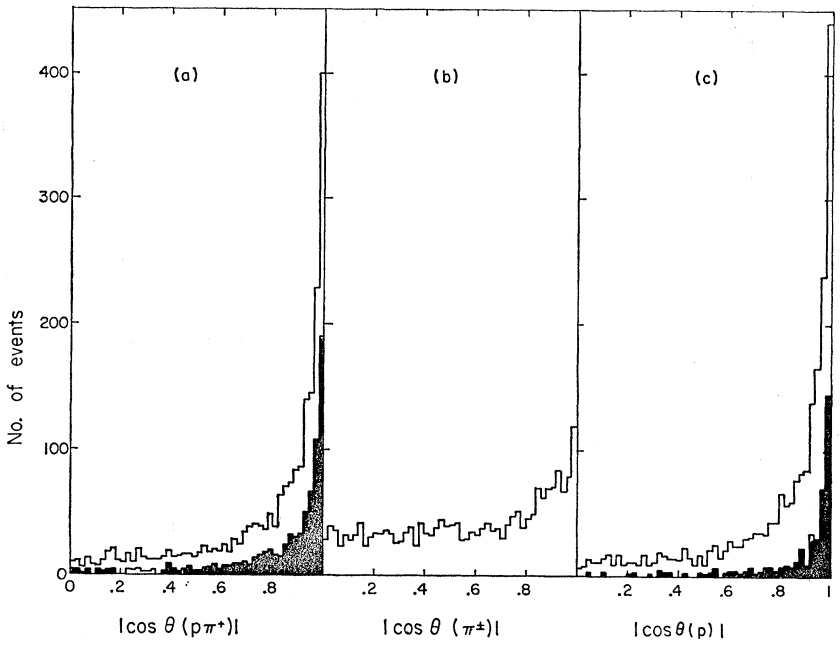

FIG. 12. Folded angular distribution of the $pp\pi^+\pi^-$ final-state particles. Shaded area in (a): events belonging to $N^*_{1238}(p\pi^+)$; in (c): events belonging to $N^*_{1518}\times(p\pi^+\pi^-)$ and $N^*_{1688}(p\pi^+\pi^-)$.

fit of $A=2.96\pm0.58$ mb/(GeV/c)^2 and $b=15.8\pm2.9$ (GeV/c)$^{-2}$ were then assumed to hold for the full kinematically possible Δ^2 region, yielding a cross section of $\sigma(pp\to N^*_{1238}p)=0.376\pm0.076$ mb. These results may be compared with the present results of $pp\to N^*_{1238}p$ at 5.5 GeV/c. Using a similar Δ^2 region of 0.02 to 0.11 (GeV/c)^2 for the $N^*_{1238}(p\pi^+)$ data we multiplied the resulting cross sections by the isospin-predicted ratio of $\sigma(pp\to N^*_{1238}p)/\sigma(pp\to N^*_{1238}n)=\frac{1}{3}$. In this way we have obtained $A=4.68\pm1.1$ mb/(GeV/c)^2 and $b=(12.3\pm3.5)$ (GeV/c)^2, corresponding to a cross-section value of $\sigma(pp\to N^*_{1238}p)=0.76\pm0.30$ mb. This last value is lower than the value 1.08 ± 0.05 mb deduced from the invariant-mass-distribution study of N^{*++}_{1238} with the same division by 3 (see Table III).

VI. THE REACTION $pp\to pp\pi^+\pi^-$

The reaction (4) in Table I, $pp\to pp\pi^+\pi^-$, was studied in a sample of 1050 uniquely identified events. The c.m. angular distribution (folded around 90°) of the proton produced in this reaction is given in Fig. 12, where each event contributes twice to the histogram. The protons are strongly peaked backward, and forward along the incident-particle direction, with a median angle of $\cos\theta=0.9$, suggesting a peripheral production mechanism. The pions, on the other hand, are more isotropically distributed, with some peaking in the $|\cos\theta|>0.8$ cone [Fig. 12(b)].

Information about resonance production in the final state $pp\pi^+\pi^-$ can be obtained from a study of the invariant-mass distributions of its various particle combinations. Invariant-mass histograms of the two- and three-particle configurations of the reaction (4) are shown in Fig. 13. Each invariant-mass histogram is compared with its appropriate phase-space distribution (dashed line). Deviations from the phase-space distribution are found in all invariant-mass histograms; in particular, they are obvious in $M(p\pi^+\pi^-)$, $M(p\pi^+)$, and $M(p\pi^-)$. In these histograms there are indications for the production of the isobars: $N^*_{1238}(p\pi^+)$, $N^*_{1518}(p\pi^+\pi^-)$, and $N^*_{1688}(p\pi^+\pi^-)$.

Best-fit calculations using all the events show that all six histograms in Fig. 13 may be explained in a consistent way by the same mixture of channels. The cross-section values of the different channels are summarized in Table IV. The peripheral nature of the interactions, the correlations between the different channels, and the

TABLE IV. Partial cross sections of channels contributing to the $pp\pi^+\pi^-$ final state. Errors quoted are from best-fit procedure only.

	Channel	Cross section (mb)
A	$N^*_{1518}(p\pi^+\pi^-)p$	0.57 ± 0.05
B	$N^*_{1688}(p\pi^+\pi^-)p$	0.48 ± 0.04
C	$N^*_{1920}(p\pi^+\pi^-)p$	0.42 ± 0.06
D	$N^*_{2360}(p\pi^+\pi^-)p$	~0
E	$N^*_{1238}(p\pi^+)p\pi^-$	0.28 ± 0.04
F	$N^*_{1238}(p\pi^+)N^*_{1238}(p\pi^-)$	0.25 ± 0.04
G	$N^*_{1238}(p\pi^+)N^*_{1420}(p\pi^-)$	0.13 ± 0.04
H	$N^*_{1238}(p\pi^+)N^*_{1518}(p\pi^-)$	0.02 ± 0.02
I	$N^*_{1238}(p\pi^+)N^*_{1688}(p\pi^-)$	0.21 ± 0.04
J	$N^*_{1238}(p\pi^-)p\pi^+$	0.12 ± 0.01
K	$N^*_{1420}(p\pi^-)p\pi^+$	0.04 ± 0.01
L	$N^*_{1518}(p\pi^-)p\pi^+$	0.08 ± 0.02
M	$N^*_{1688}(p\pi^-)p\pi^+$	0.02 ± 0.02
N	$pp\rho_{763}(\pi^+\pi^-)$	0.07 ± 0.05
O	$pp\pi^+\pi^-$	~0

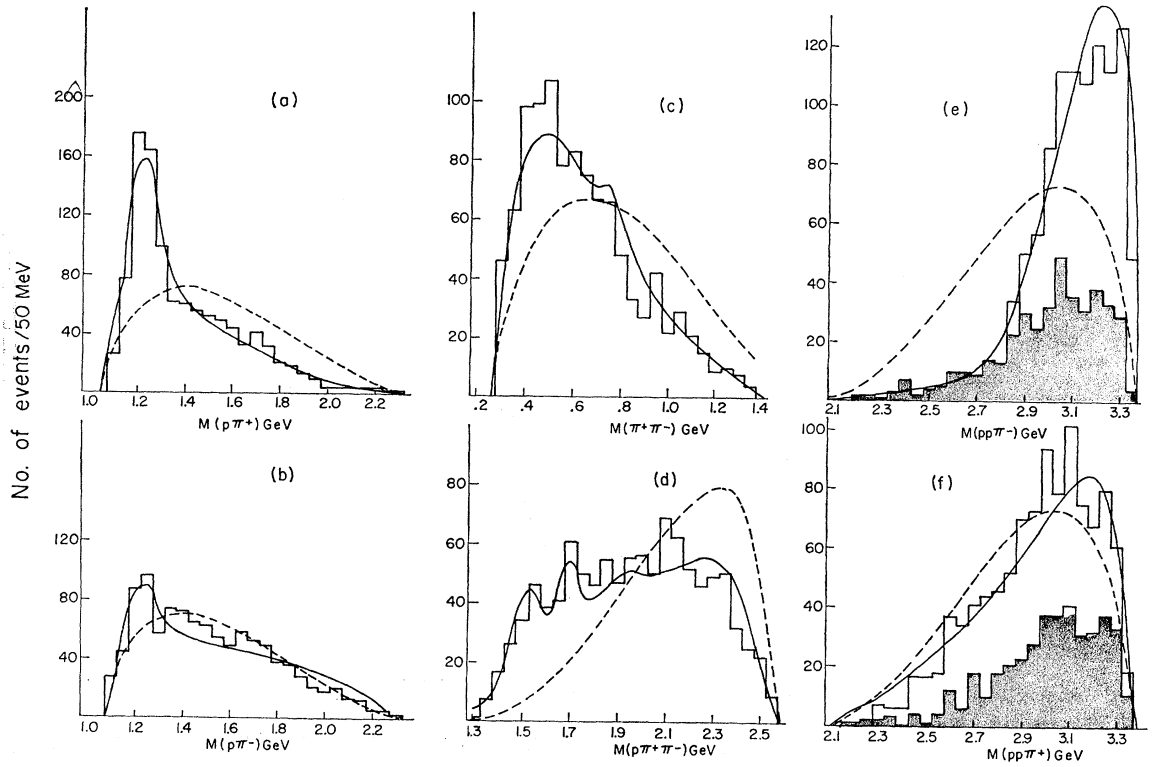

FIG. 13. Various invariant-mass histograms in the $pp\pi^+\pi^-$ final state. Shaded area includes events outside $N^*_{1238}(p\pi^+)$ region.

detailed study of the different channels contributing to the reaction $pp \to pp\pi^+\pi^-$ are discussed in the next sections.

A. The $p\pi^+\pi^-$ Combination

The angular distribution of the three-particle combination $p\pi^+\pi^-$, which is equivalent to the proton angular distribution, shown in Fig. 12(c), is limited to a narrow cone around the incident direction indicating very peripheral production. The c.m. angular distribution of the $p\pi^+\pi^-$ combination associated with the isobars $N^*_{1518}(p\pi^+\pi^-)$ and $N^*_{1688}(p\pi^+\pi^-)$, shown by the shaded area in Fig. 12(c), is somewhat more forward-backward peaked than that of the rest of the events. This fact indicates that the $N^*_{1518}(p\pi^+\pi^-)$ and $N^*_{1688}(p\pi^+\pi^-)$ are pheripherally produced in the reactions $pp \to N^* + p$. This peripheral nature may be used to resolve the ambiguity between the proton belonging to the isobar (p_1) and the other proton (p_2). To this end, the invariant mass $M(p\pi^+\pi^-)$ was plotted as follows: first, for small $[\Delta^2(p_1\pi^+\pi^-) < 0.45\ (\mathrm{GeV}/c)^2]$ and large $[\Delta^2(p_2\pi^+\pi^-) > 0.45\ (\mathrm{GeV}/c)^2]$ momentum transfer, as shown in Figs. 14(a) and (b); and second, only the $p\pi^+\pi^-$ combination in each event which had the smaller momentum transfer (DMD method), as shown in Fig. 14(c).

The results of the best fit to these histograms are shown as the solid lines in Fig. 14(a), (b), and (c). It appears that the separation between combinations with small and large momentum transfer is quite effective for the distinction between the proton belonging to the isobar (p_1) and the other proton (p_2). In fact the small-$\Delta^2(p_1\pi^+\pi^-)$ histogram is well accounted for by the invariant-mass distribution of $N^*_{1238}(p\pi^+)\pi^-$, $N^*_{1518}(p\pi^+\pi^-)$, and $N^*_{1688}(p\pi^+\pi^-)$; while the large-$\Delta^2(p_2\pi^+\pi^-)$ mass histogram is explained by the reflection of the same contributions. There is a general agreement between the best-fit results to the $M(p\pi^+\pi^-)$ histogram displayed in the different methods. The most probable mixture of channels is summarized in terms of cross-section values in Table IV.

In Fig. 14(d) the $M(p\pi^+\pi^-)$ distribution is shown for those events where $M(p\pi^+)$ is in the $N^*_{1238}(p\pi^+)$ region, that is $1175 \leqslant M(p\pi^+) \leqslant 1305$ MeV. The solid line in the same figure represents the best fit to the data indicating the production of the three isobars: $N^*_{1518}(p\pi^+\pi^-) \sim 20\%$; $N^*_{1688}(p\pi^+\pi^-) \sim 20\%$, and $N^*_{1920}(p\pi^+\pi^-) \sim 10\%$. The appearance of heavy isobars in the $N^*_{1238}(p\pi^+)\pi^-$ mass histogram suggests that part of the production of $N^*_{1238}(p\pi^+)$ is in fact a decay product of these heavier isobars $N^*(p\pi^+\pi^-) \to N^*_{1238}(p\pi^+)\pi^-$. To study this possibility, the invariant mass $M(p\pi^+)$ was plotted for events belonging to different $M(p\pi^+\pi^-)$ regions. The $M(p\pi^+)$ histogram for events in the region $1460 \leqslant M(p\pi^+\pi^-) \leqslant 1580$ MeV fits well both the $p\pi^+$ phase-space distribution, and a Breit-Wigner–type curve of the $N^*_{1238}(p\pi^+)$ isobar. It is for this reason that we were unable to estimate the decay rate of $N^*_{1518}(p\pi^+\pi^-) \to N^*_{1238}(p\pi^+)\pi^-$.

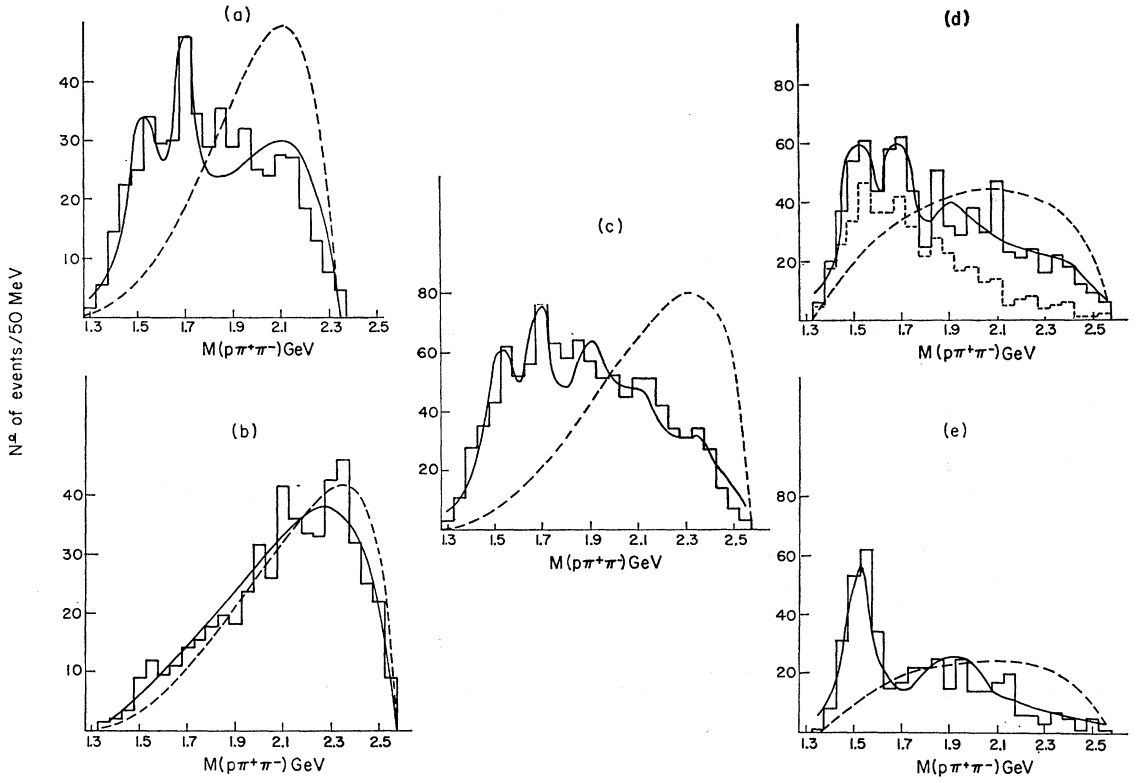

FIG. 14. Invariant-mass distributions of $p\pi^+\pi^-$ in the $pp\pi^+\pi^-$ final state for (a) events with $\Delta^2(p\pi^+\pi^-)<0.45$ GeV^2, (b) events with $\Delta^2(p\pi^+\pi^-)>0.45$ GeV^2, (c) all events, chosen with the DMD method, (d) events with $M(p\pi^+)$ in the $N^*_{1238}(p\pi^+)$ region [broken line: DMD of $M(p_1\pi^+\pi^-)$], and (e) events with $M(p\pi^-)$ in the $N^*_{1238}(p\pi^-)$ region.

The histogram of $M(p\pi^+)$ in the region $1640\leqslant M(p\pi^+\pi^-)\leqslant 1740$ MeV clearly shows $N^*_{1238}(p\pi^+)$ formation. The best fit to this $M(p\pi^+)$ histogram yields $(67\pm3)\%$ $N^*_{1238}(p\pi^+)$ and $(33\pm3)\%$ phase-space distributions. This result was then used to obtain a branching value of

$$R=\frac{\Gamma[N^*_{1688}(p\pi^+\pi^-)\rightarrow N^*_{1238}(p\pi^+)\pi^-]}{\Gamma[N^*_{1688}(p\pi^+\pi^-)\rightarrow p\pi^+\pi^-(\text{all modes})]}=0.74\pm0.14$$

after the following facts had been taken in account: (a) Only about 50% of the events with $1.64\leqslant M(p\pi^+\pi^-)\leqslant 1.74$ GeV are decay products of the $N^*_{1688}(p\pi^+\pi^-)$ isobar, and (b) an additional 30% of the events are associated with a directly produced $N^*_{1238}(p\pi^+)$ isobar in the $M(p\pi^+)$ histogram.

A similar value for this branching ratio was obtained in a second independent way. For a branching-ratio value R, the fraction $F(R)$ of $N^*_{1688}(p\pi^+\pi^-)$ decay events lying inside the region of $1.175\leqslant M(p\pi^+)\leqslant 1.305$ GeV is given by $F(R)=(1-R)F(0)+RF(1)$; where $F(0)=0.31$ for pure phase space (spin effects were neglected), and $F(1)=0.594$ for pure $N^*_{1688}\rightarrow N^*_{1238}\pi$ decay. The best fit to the experimental $M(p_1\pi^+\pi^-)$ invariant-mass histogram (a) of all events and (b) only of events with $1.175\leqslant M(p_1\pi^+)\leqslant 1.305$ GeV, both chosen with the DMD method, are shown in Fig. 14(c) and 14(d) (dashed lines). These fits yielded a value of $F=0.52\pm0.11$ for the fraction of $N^*_{1688}(p\pi^+\pi^-)$ events with $1.175\leqslant M(p_1\pi^+)\leqslant 1.305$ GeV, which in turn determines the branching ratio to be $R=0.7\pm0.4$.

The situation with regard to the production of $N^*_{1920}(p\pi^+\pi^-)$ is somewhat less certain. In Fig. 13(d) no enhancement above background is seen in the region of 1.92 GeV; on the other hand, the best fit to the data of events, DMD-selected events, and $N^*_{1238}\pi^-$ selected events yield large values of 15%, 20%, and 10%, respectively, for the $N^*_{1920}(p\pi^+\pi^-)$ production. At the same time the data are consistent with no $N^*_{2360}(p\pi^+\pi^-)$ production.

B. The $p\pi^+$ and $p\pi^-$ Configurations

The $M(p\pi^+)$ invariant-mass histogram shown in Fig. 13(a) is consistent with about 60% $N^*_{1238}(p\pi^+)$ isobar production. It has been shown previously that part of this $N^*_{1238}(p\pi^+)$ is contributed from the decay of heavy isobars. The invariant-mass histogram of $M(p\pi^-)$ shown in Fig. 13(b) is different from that of $M(p\pi^+)$. The $N^*_{1238}(p\pi^-)$ is less pronounced, and there are slight enhancements in the regions of the $N^*_{1420}(p\pi^-)$, $N^*_{1518}(p\pi^-)$, and $N^*_{1688}(p\pi^-)$ isobars above the best-fit curve of the main isobar channels in Table IV. With the aid of the best-fit curves to the invariant-mass histograms $M(p\pi^+\pi^-)$, it was estimated that in about 50% of the

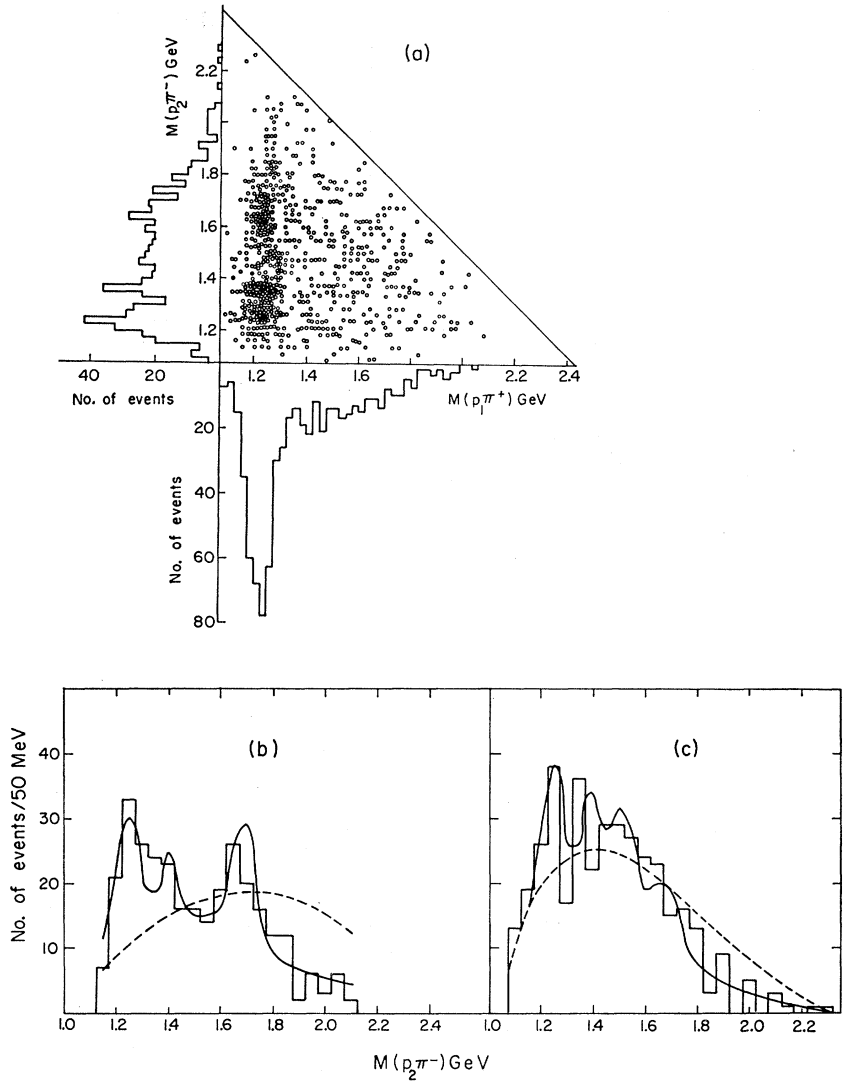

FIG. 15. Invariant-mass distributions in the $pp\pi^+\pi^-$ final state. (a) $M(p_1\pi^+)$ versus $M(p_2\pi^-)$; (b) and (c): $M(p_2\pi^-)$ histograms for events with $M(p_1\pi^+)$ inside and outside $N^*_{1238}(p\pi^+)$ region.

$pp \to pp\pi^+\pi^-$ events, either $N^*_{1238}(p\pi^+)$ or $N^*_{1238}(p\pi^-)$ isobars were directly produced.

The angular distribution of the $p\pi^+$ configuration is shown in Fig. 12(a). The strong forward-backward peaking of the shaded area in this figure, which belongs to events with invariant mass lying inside the N^*_{1238}-$(p\pi^+)$ region, suggests a peripheral production of the $N^*_{1238}(p\pi^+)$. The direct production of $N^*_{1238}(p\pi^+)$ was further studied in an enriched sample from which all events associated with either $N^*_{1518}(p\pi^+\pi^-)$ or N^*_{1688}-$(p\pi^+\pi^-)$ were removed. The ambiguity of the two final-state protons was resolved by the minimal-momentum-transfer method described earlier (DMD). Finally the triangle plot of $M(p\pi^+)$ versus $M(p\pi^-)$ is shown in Fig. 15(a). There is a concentration of events in the N^*_{1238}-$(p\pi^+)$ band. The $M(p\pi^-)$ histograms of events with $M(p\pi^+)$ inside and outside the $N_{1238}(p\pi^+)$ band, together with their best-fit curves, are presented in Figs. 15(b) and (c), respectively. From the study of $M(p\pi^+)$ and $M(p\pi^-)$ in the different methods described above, the cross sections for various direct $N^*(N\pi)$ productions were estimated, and they are given in Table IV.

C. The $\pi^+\pi^-$ Configuration

The general shape of the $M(\pi^+\pi^-)$ histogram is well explained by the mixture of isobars channels listed in Table IV. The best fit to the data in Fig. 13(c) yields a ρ-meson production cross section of 0.07 ± 0.05 mb. A partial sample, from which all events associated with $N^*_{1238}(p\pi^+)$, $N^*_{1518}(p\pi^+\pi^-)$, and $N^*_{1688}(p\pi^+\pi^-)$ were omitted, yielded the same small amount of ρ production. Thus one may conclude that there is very little ρ production in the $pp \to pp\pi^+\pi^-$ reaction.

D. The $pp\pi^+$ and $pp\pi^-$ Configurations

The invariant-mass histograms of the two possible $B=2$ combinations $pp\pi^+$ and $pp\pi^-$ are well described

by the isobar channels dealt with earlier [see Figs. 13(e) and (f)]. There is no evidence for the production of a $B=2$ resonance state in the present experiment. In particular we can put an upper limit of 0.06 mb on the possible $pp\pi^+$ state at $M=2.52$ GeV reported by Kidd *et al.*[10]

VII. THE REACTION $pp \to np\pi^+\pi^-\pi^+$

The reaction $pp \to np\pi^+\pi^-\pi^+$ was studied with a sample of 960 uniquely identified events. The c.m. angular distributions of the nucleons and pions produced in this reaction are given in Fig. 16. The angular distributions of the $N\pi$ combinations are very similar to those of the proton and the neutron. The angular distribution of the pions is nearly isotropic.

The ambiguity between the two π^+ mesons in the $np\pi^+\pi^-\pi^+$ final state may be resolved by choosing as the "right" pion, π_1^+, the one with the minimum momentum transfer (DMD) i.e., $\Delta^2(p\pi_1^+)<\Delta^2(p\pi_2^+)$. The angular distribution of the "right" $p\pi_1^+$ combination is more peaked in the forward-backward direction (with a median of $|\cos\theta| = 0.88$) than the angular distribution of the protons alone (with a median of $|\cos\theta| = 0.83$).

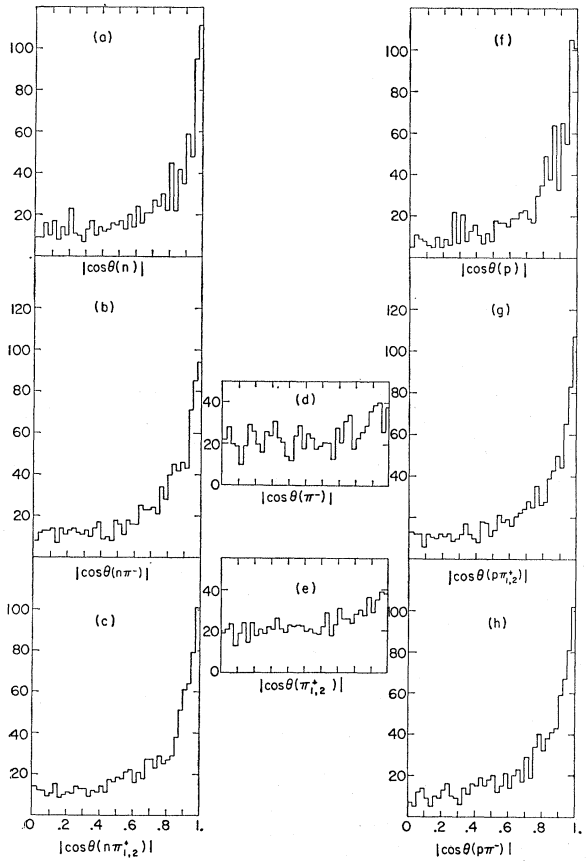

FIG. 16. Folded angular distributions of the $np\pi^+\pi^+\pi^-$ final-state particles.

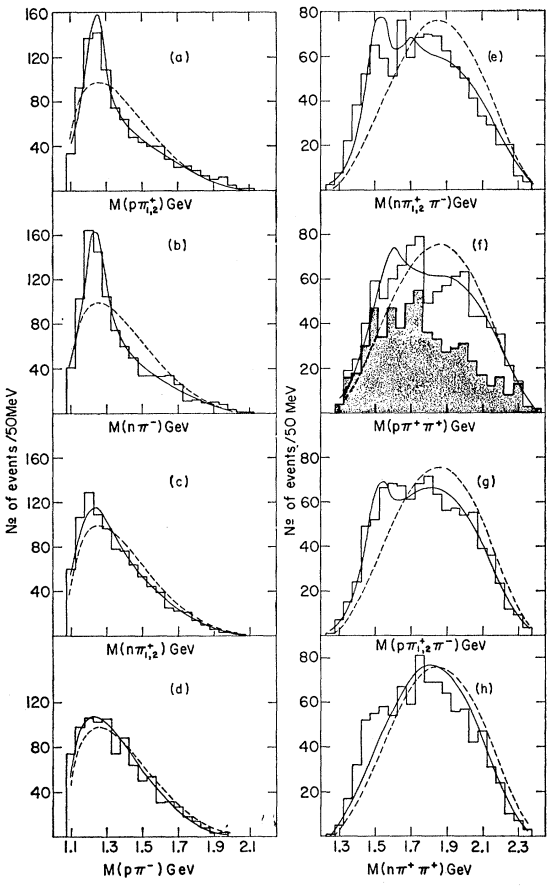

FIG. 17. Invariant-mass distributions of various $np\pi^+\pi^+\pi^-$ final-state configurations. The shaded area in (f) includes all events with $M(n\pi^-)$ outside the $N^*_{1238}(n\pi^-)$ region.

A. Production of the $N^*_{3/2}(1238)$ Isobar

The invariant-mass histograms of the various nucleon-pion combinations in the final state $np\pi^+\pi^+\pi^-$ are plotted in Fig. 17. The best-fit analysis of the $p\pi^+$ and $n\pi^-$ configurations show appreciable production of the isobar states $N^*_{1238}(p\pi^+)$ and $N^*_{1238}(n\pi^-)$. On the other hand, the best-fit solution of the $p\pi^-$ histogram gave zero $N^*_{1238}(p\pi^-)$ isobar production, while the $n\pi^+$ fit yielded 5% $N^*_{1238}(n\pi^+)$ in the final state $np\pi^+\pi^-\pi^+$.

The correlation between the two isobar states N^*_{1238}-$(p\pi^+)$ and $N^*_{1238}(n\pi^-)$ was studied by a triangle plot of $M(p\pi^+_1)$ versus $M(n\pi^-)$ (see Fig. 18), where the $p\pi_1^+$ combinations were chosen by the DMD method. This plot shows evidence for double isobar production: $pp \to N^*_{1238}(p\pi^+)+N^*_{1238}(n\pi^-)+\pi^+$.

The amounts of $N^*_{1238}(p\pi^+)$ and $N^*_{1238}(n\pi^-)$ found by the best-fit analysis of the various $p\pi^+$ and $n\pi^-$ histograms (see Fig. 19) are: $\sigma(N^*_{1238}(p\pi^+)n\pi^+\pi^-) = 1.44\pm0.25$ mb, $\sigma(N^*_{1238}(p\pi^+)N^*_{1238}(n\pi^-)\pi^+) = 0.75 \pm 0.16$ mb, and $\sigma(N^*_{1238}(n\pi^-)p\pi^+\pi^-) = 0.22+0.15$ mb. These total cross sections include some contributions from the decay of heavier isobars like $N^*_{1518}(p\pi^+\pi^-)$ and $N^*_{1518}(n\pi^+\pi^-)$.

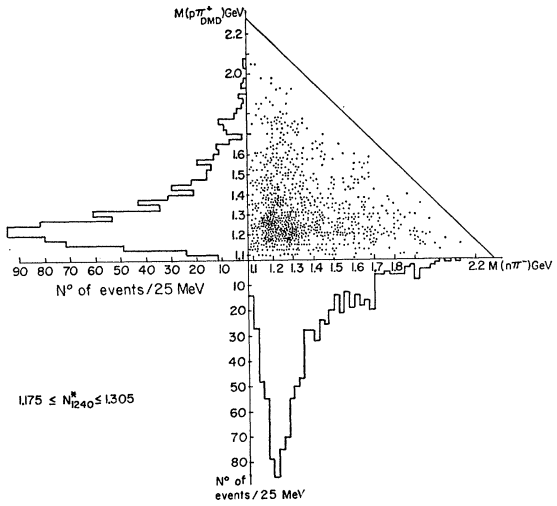

FIG. 18. Plot of $M(n\pi^-)$ versus $M(p\pi^+)$ in the final state $np\pi^+\pi^+\pi^-$. The $p\pi^+$ combination was chosen with the DMD method (see text).

B. Production of the $N^*_{1518}(p\pi^+\pi^-)$ and $N^*_{1518}(n\pi^+\pi^-)$ Isobar States

The invariant-mass histogram of $M(p\pi^+\pi^-)$ with both π^+ meson combinations, was used to study the amount of the $N^*_{1518}(p\pi^+\pi^-)$ and $N^*_{1688}(p\pi^+\pi^-)$ in the final state $np\pi^+\pi^-\pi^+$. The best-fit analysis yields 25% $N^*_{1518}(p\pi^+\pi^-)$ production (see channel I in Table V) and practically zero $N^*_{1688}(p\pi^+\pi^-)$ production.

The cross-section values for the $N^*_{1518}(n\pi^-\pi^+)$ production (channels B and G in Table V) were obtained through the best-fit method to the $M(n\pi^+\pi^-)$ mass histograms displayed in three different ways: (a) using only events with $M(n\pi^-)$ inside the $N^*_{1238}(n\pi^-)$ band, (b) using events with $M(p\pi^+)$ outside the $N^*_{1238}(p\pi^+)$ band, and (c) using events with $M(p\pi^+)$ inside the $N^*_{1238}(p\pi^+)$ band (Fig. 20).

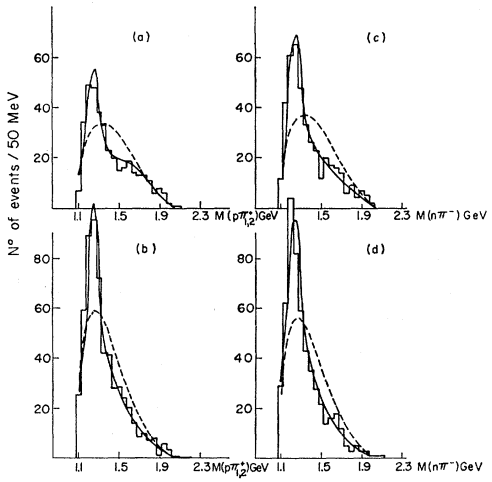

FIG. 19. Two-body invariant-mass distributions of the $np\pi^+\pi^+\pi^-$ final state. (a) $p\pi^+_{1,2}$ for events inside and (b) outside $N^*_{1238}(n\pi^-)$ region; (c) $n\pi^-$ for events inside and (d) outside $N^*_{1238}(p\pi^+)$ region.

The cross sections for direct $N^*_{1238}(p\pi^+)n\pi^+\pi^-$ and $N^*_{1238}(p\pi^+)N^*_{1238}(n\pi^-)\pi^+$ production listed in Table V (channels A and D) were obtained after the contributions from heavier isobar decays (channel G in Table V) were substracted from their respective total values obtained from the $p\pi^+$ and $n\pi^-$ histograms in the previous section. At the same time the cross section of $N^*_{1518}(n\pi^-\pi^+)$ (channel G, Table V) account for all the amount of $N^*_{1238}(n\pi^-)p\pi^+\pi^+$ found in the $n\pi^-$ invariant-mass histogram, and it is consistent with no direct production of $N^*_{1238}(n\pi^-)p\pi^+\pi^+$ in the pp collisions at this incident momentum.

C. The $p\pi^+\pi^+$ Combination at $M=1580$ MeV

In a previous analysis of pp interactions at 5.5 GeV/c, supporting evidence for a possible $p\pi^+\pi^+$ resonance at $M=1580$ MeV[25] was given.[2] This resonance will be discussed presently with three times as many events.

TABLE V. Partial cross sections of channels contributing to the $np\pi^+\pi^+\pi^-$ final state. Errors quoted are from best fit only.

Channel	Cross section (mb)
A $N^*_{1238}(p\pi^+)n\pi^+\pi^-$	1.02±0.15
B $N^*_{1238}(p\pi^+)N^*_{1518}(n\pi^+\pi^-)$	0.15±0.02
C $N^*_{1238}(p\pi^+)N^*_{1688}(n\pi^+\pi^-)$	0.06±0.02
D $N^*_{1238}(p\pi^+)N^*_{1238}(n\pi^-)\pi^+$	0.59±0.16
E $N^*_{1238}(n\pi^-)p\pi^+\pi^+$	~0
F $N^*_{1238}(n\pi^+)p\pi^+\pi^-$	0.17±0.06
G $N^*_{1518}(n\pi^+\pi^-)p\pi^+$	0.26±0.03
H $N^*_{1688}(n\pi^+\pi^-)p\pi^+$	0.04±0.02
I $N^*_{1518}(p\pi^+\pi^-)n\pi^+$	0.42±0.18
J $N^*_{1688}(p\pi^+\pi^-)n\pi^+$	0.07±0.02
K $np\pi^+\pi^-\pi^+$	0.24±0.03

The invariant-mass histogram of the $p\pi^+\pi^+$ combination plotted on Fig. 17(f) and shows two asymmetric enhancements with peaks around 1.7 and 2.0 GeV, respectively. The peak at 2.0 GeV is due to the reflection of the $N^*_{1238}(n\pi^-)$ found in the final state $np\pi^+\pi^-\pi^+$, and it is completely absent when all events with $1.08 \leqslant M(n\pi^-) \leqslant 1.30$ GeV are omitted from the sample [See shaded area in Fig. 17(f)].

The enhancement at 1.7 GeV could be due to the combination N^{*++}_{1238} and or the possible $p\pi^+\pi^+$ resonance at $M=1580$ MeV .The best-fit solution to this histogram yields: 30% $N^{*++}_{1238}\pi^+$ and (15±4.0)% $p\pi^+\pi^+$ resonance at $M=1580$ MeV. Attempts to fit the histogram on Fig. 17(f) without a resonance at

[25] G. Goldhaber, S. Goldhaber, T. O'Halloran, and B. C. Shen, in *Proceedings of the International Conference on High-Energy Physics, Dubna, 1964* (Atomizdat, Moscow, 1965), p. 480; G. Goldhaber, in *Proceedings of the Second Coral Gables Conference on Symmetry Particles at High-Energy*, edited by B. Kursunoglu, A. Perlmutter, and I. Sakmar (W. H. Freeman and Company, San Francisco, California, 1965).

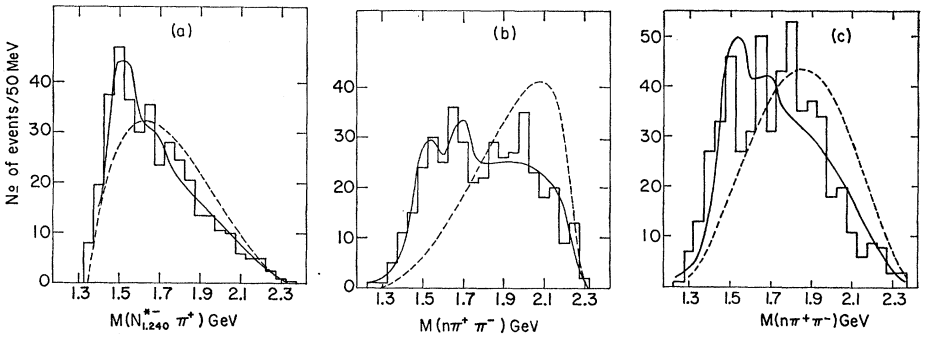

FIG. 20. Invariant-mass distributions of $n\pi_1^+\pi^-$ in the $np\pi^+\pi^+\pi^-$ final state for events (a) with $M(n\pi^-)$ in the $N^*_{1238}(n\pi^-)$ region, (b) with $M(p\pi_2^+)$ inside $N^*_{1238}\times(p\pi_2^+)$, (c) with $M(p\pi_2^+)$ outside $N_{1238}(p\pi_2^+)$.

$M(p\pi^+\pi^+)=1580$ MeV were less successful. Previous reports connected the $p\pi^+\pi^+$ resonance with small momentum transfer, and it was best observed for a sample with $\Delta^2(p\pi^+\pi^+)<0.8$ (GeV)^2. The $M(p\pi^+\pi^+)$ histogram for all events with small momentum transfer $\Delta^2(p\pi^+\pi^+)<0.8$ (GeV)^2 [see Figure 21(a)] shows a wide peak between 1.48 and 1.7 GeV. The best-fit solution for this histogram histogram yields: zero $M(p\pi^+\pi^+)=1580$-MeV resonance, and 85% $N^{*++}_{1238}\pi^+$ combination.

Finally, the relation between the possible $p\pi^+\pi^+$ resonance and the combination $N^{*++}_{1238}\pi^+$ was studied. $M(p\pi^+\pi^+)$ was plotted for all events with $1.08\leqslant M(p\pi^+)\leqslant 1.30$ [see Fig. 21(b)]. The best fit to this histogram yields zero 1580-MeV resonance and 70% $N^{*++}_{1238}\pi^+$ combination.

We may conclude that the analysis of the present data of the $np\pi^+\pi^+\pi^-$ final state does not provide sufficient evidence to prove the existence of a new $p\pi^+\pi^+$ resonance at $M=1580$ MeV.

D. Other Combinations of Nucleons and Pions

The invariant-mass histograms of the combinations $n\pi^+\pi^+$, $pn\pi^+$, $pn\pi^-$, $p\pi^+\pi^-\pi^+$, and $n\pi^+\pi^-\pi^+$ were studied. The best-fit solutions of these histograms agree in general with phase-space distributions, together with the isobar channels found in the reaction $pp\rightarrow np\pi^+\pi^-\pi^+$ as listed in Table V. No evidence for new isobar states was found in these histograms.

The invariant-mass histograms of two- and three-pion combinations [Figs. 22(a) and 22(b)] in the final state $np\pi^+\pi^-\pi^+$ did not show any evidence for a mesonic resonance. The best-fit solutions to these histograms were consistent with reflections of the N^{*++}_{1238} and N^{*-}_{1238} isobars.

Finally, the cross section for the nonresonance final state (i.e., phase space) is $\sigma(np\pi^+\pi^-\pi^+)=0.25\pm0.03$ mb (listed in Table V channel K) was found by subtracting the cross section values of all the main isobar channels from the total $pp\rightarrow np\pi^+\pi^-\pi^+$ cross section of 2.85 ±0.08 mb.

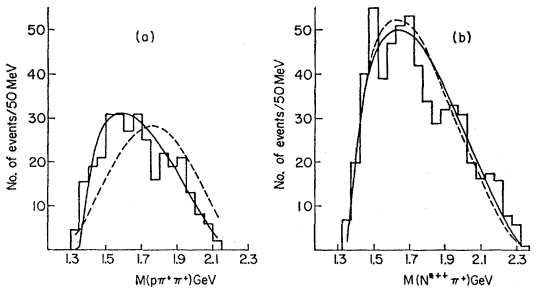

FIG. 21. Invariant-mass histograms of the $p\pi^+\pi^+$ configuration in the $np\pi^+\pi^+\pi^-$ final state, for events with (a) $\Delta^2(p\pi^+\pi^+)<0.8$ (GeV)^2 and (b) $M(p\pi^+)$ in the $N^*_{1238}(p\pi^+)$ region.

VIII. THE REACTION $pp\rightarrow pp\pi^+\pi^0\pi^-$

The reaction $pp\rightarrow pp\pi^+\pi^0\pi^-$ was studied in a sample of 620 uniquely identified events. The c.m. angular distribution of the proton in the final state $pp\pi^+\pi^0\pi^-$ [see Fig. 23(a)] is peaked in the forward-backward direction with a median of $|\cos\theta|=0.83$. The pions (π^+,π^0,π^-) in the same final state have almost isotropic c.m. angular distribution [see Figs. 23(b), 23(c), and 23(d)]. The nucleon-pion combinations [see Figs. 23(e), 23(f), and 23(g)] are also peaked in the forward-backward direction, but slightly less so than the protons alone. The $p\pi^+$,

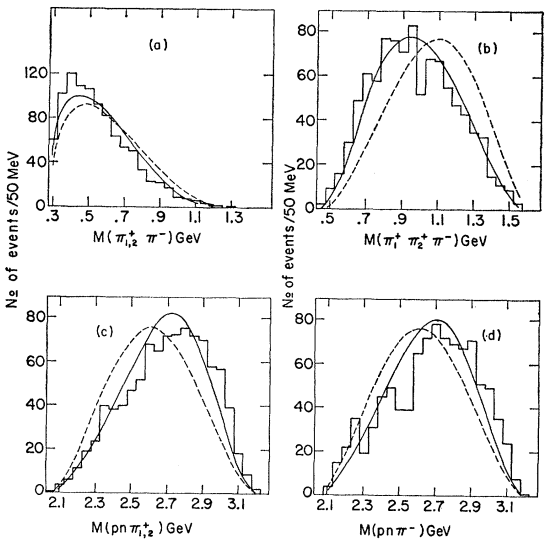

FIG. 22. Invariant-mass distributions of $np\pi^+\pi^+\pi^-$ final-state configurations.

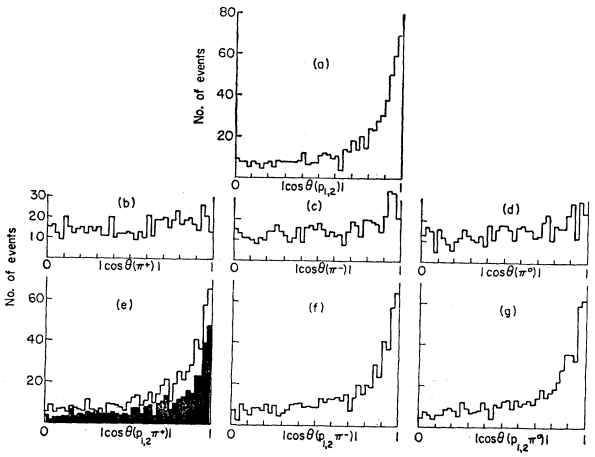

FIG. 23. Folded angular distributions of the $pp\pi^+\pi^-\pi^0$ final-state particles. Shaded area in (e) includes only events belonging to $N^*_{1238}(p\pi^+)$.

$p\pi^0$, and $p\pi^-$ configurations have similar angular distributions with the same median $|\cos\theta| = 0.79$. Finally the $p\pi^+$ configuration, in the N^*_{1238}-isobar mass region, has angular distribution [see shaded area in Fig. 23(e)] like that of the protons, with a median $|\cos\theta| = 0.83$.

An attempt was made to resolve the double-proton ambiguity in the final state $pp\pi^+\pi^0\pi^-$ by choosing the "right" proton by its "right" $p_1\pi^+$ combination through the DMD method $\Delta^2(p_1\pi^+) < \Delta^2(p_2\pi^+)$. The angular distribution of the combination $p_1\pi^+$ so chosen is more peaked than that of all the protons, with a median $|\cos\theta| = 0.88$.

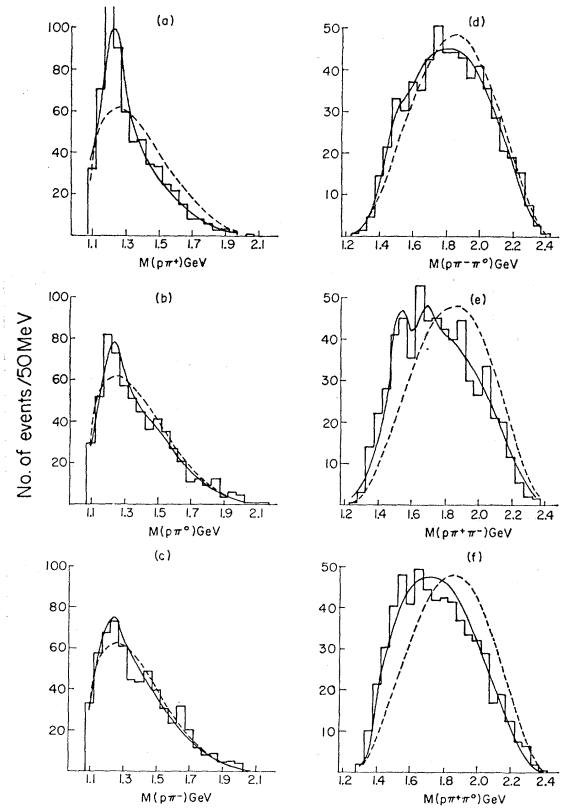

FIG. 24. Various invariant-mass distributions of $pp\pi^+\pi^-\pi^0$ final-state configurations.

A. $N\pi$ Configuration

The $M(p_{1,2}\pi^+)$, $M(p_{1,2}\pi^0)$, and $M(p_{1,2}\pi^-)$ invariant-mass histograms show peaks in the 1.240-GeV region. The best-fit calculations yield 60% $N^*_{1238}(p\pi^+)$, 35% $N^*_{1238}(p\pi^0)$, and 19% $N^*_{1238}(p\pi^-)$ for each histogram, respectively, (Fig. 24).

Some of the events have double isobars in their final state. In order to study the double-isobar events, the invariant masses $M(p_2\pi^0)$, $M(p_2\pi^-)$, and $M(p_2\pi^0\pi^-)$ were plotted for events with $1.175 \leqslant M(p_1\pi) \leqslant 1.305$ GeV [see Figs. 25(a), 25(b), (25(c)]. The best-fit results show evidence for double-isobar final states such as $N^*_{1238}(p\pi^+)N^*_{1238}(p\pi^0)\pi^-$, and $N^*_{1238}(p\pi^+)N^*_{1238}(p\pi^-)\pi^0$, and also very small amounts of $N^*_{1238}(p\pi^+)N^*_{1518}(p\pi^0)\pi^-$ and $N^*_{1238}(p\pi^+)N^*_{1518}(p\pi^-)\pi^0$. At the same time, the

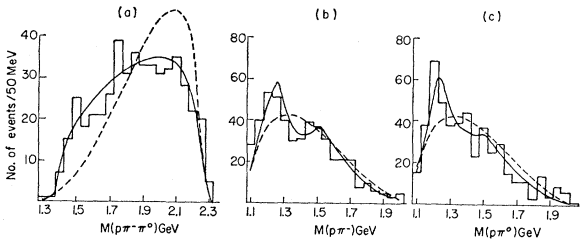

FIG. 25. Various invariant-mass distributions of $pp\pi^+\pi^-\pi^0$ final-state configurations. (a) $p_2\pi^-\pi^0$, (b) $p_2\pi^-$, (c) $p_2\pi^0$ for events with $M(p_1\pi^+)$ inside $N^*_{1238}(p_1\pi^+)$ region.

results did not show any contribution of the final state $N^*_{1238}(p\pi^+)N^*_{1518}(p\pi^0\pi^-)$.

The cross sections for the different charge states of the N^*_{1238} isobar deduced from the best fits described in this chapter include some contributions from the decay of heavier isobars like $N^{*+}_{1520} \rightarrow p\pi^+\pi^-$. At the same time, the N^*_{1238} cross sections are not mutually exclusive, and in some events the same proton appears simultaneously with the π^+ and the π^0 in the N^*_{1238} mass region.

B. The $N\pi\pi$ Configuration

The invariant-mass histograms of the three possible $N\pi\pi$ configurations $M(p\pi^-\pi^0)$, $M(p\pi^+\pi^-)$, and $M(p\pi^+\pi^0)$ are plotted in Fig. 24. Both $M(p\pi^+\pi^-)$ and $M(p\pi^+\pi^0)$ histograms show enhancements above the phase-space distribution in the 1.4- 1.7- GeV region, while the $M(p\pi^0\pi^-)$ histogram deviates slightly from phase-space distribution in the vicintiy of $M = 1.520$ GeV.

The best-fit solutions show production of the N^*_{1518} in the two channels $pp \rightarrow N^*_{1518}(p\pi^+\pi^-)p\pi^0$ (24%) and

$pp \to N^*_{1518}(p\pi^0\pi^-)p\pi^+$ (6%). The production of the N^*_{1688} isobar in similar channels is smaller: 9% $N_{1688}{}^*$-$(p\pi^+\pi^-)$ and 1% $N^*_{1688}(p\pi^0\pi^-)$, respectively. The shape of the $M(p\pi^+\pi^0)$ histogram is explained by the reflections of the two isobar channels $pp \to N^*_{1238}(p\pi^+)p\pi^0\pi^-$ and $pp \to N^*_{1238}(p\pi^0)p\pi^+\pi^-$.

Best-fit solutions were found also for the histograms of $M(p_1\pi^+\pi^-)$ and $M(p_2\pi^0\pi^-)$ with $\Delta^2(p_1\pi^+) < \Delta^2(p_2\pi^+)$ (DMD method). The results obtained in this way are consistent with those mentioned above. Cross sections obtained from the fitting analysis of the $M(p\pi^+\pi^-)$ and $M(p\pi^-\pi^0)$ invariant-mass histograms are given in Table VI.

C. Mesonic Resonances

The invariant-mass histograms of the two-pion configurations $M(\pi^+\pi^0)$, $M(\pi^+\pi^-)$, and $M(\pi^0\pi^-)$ [see Figs. 26(a), 26(b), and 26(c)] do not show any clear evidence for ρ production (see Table VI).

The general shape of these histograms is well fitted by reflection distributions of the isobars found in the final state $pp\pi^+\pi^0\pi^-$.

The invariant-mass histogram for the three-pion configuration $M(\pi^+\pi^0\pi^-)$ shows a peak at 780 MeV. The best fit yields (6 ± 1)% for the ω^0 meson with $M_{\omega^0}=783$ MeV and $\Gamma_{\omega^0}=30$ MeV. The large width of the ω^0 used in the fit is due to the experimental resolution. The ω^0 production cross section with the subsequent $\omega^0 \to \pi^+\pi^0\pi^-$ decay mode is $\sigma(pp \to pp\omega^0)=110\pm20$ μb.

The $M(\pi^+\pi^-\pi^0)$ histogram [see Fig. 26(d)] also shows some indication for very small η^0 production in the reaction $pp \to pp\eta^0 \to pp\pi^+\pi^0\pi^-$ (see Table VI).

D. Partial Cross Sections

The various cross-section values that were deduced from the best-fit analysis of the different invariant-mass histograms of the final state $pp\pi^+\pi^0\pi^-$ are given in Table VI.

All the resonance cross sections listed in Table VI, except those with a single $N^*_{3/2}(1238)$ isobar (channels A, E and F), were found independently from best-fit solutions of the invariant-mass histograms of their own decay configurations. The total cross sections for the three charge states of the $N^*_{3/2}(1238)$ isobar in the final state $pp\pi^+\pi^0\pi^-$ were found by similar fits, and they are: $\sigma(N^*_{1238}(p\pi^+))=1.08\pm0.13$ mb, $\sigma(N^*_{1238}(p\pi^0))=0.64\pm0.13$ mb and $\sigma(N^*_{1238}(p\pi^-))=0.35\pm0.02$ mb. These cross sections include contributions from the decay of N^*_{1518} isobars, as well as single and double N^*_{1238} production. The cross sections for direct production of single N^*_{1238} isobars (channels A, E, and F in Table VI) were found by appropriate subtractions.

The cross sections for the mesonic resonances ω^0 and η^0 were found by independent fitting of the $M(\pi^+\pi^0\pi^-)$ invariant-mass histogram. The partial cross section for nonresonance (phase-space) production, i.e., $pp \to pp\pi^+\pi^0\pi^-$, was found by subtracting the main-resonance cross sections from the total $\sigma(pp\pi^+\pi^0\pi^-)$ final-state cross section. The errors for the resonance cross sections are the best-fit errors.

TABLE VI. Partial cross sections of channels contributing to the $pp\pi^+\pi^-\pi^0$ final state. Errors quoted are from best-fit procedure only.

	Channel	Cross section (mb)
A	$N^*_{1238}(p\pi^+)p\pi^-\pi^0$	0.20±0.02
B	$N^*_{1238}(p\pi^+)N^*_{1518}(p\pi^-\pi^0)$	~0
C	$N^*_{1238}(p\pi^+)N^*_{1238}(p\pi^0)\pi^-$	0.26±0.05
D	$N^*_{1238}(p\pi^+)N^*_{1238}(p\pi^-)\pi^0$	0.26±0.06
E	$N^*_{1238}(p\pi^0)p\pi^+\pi^-$	0.30±0.03
F	$N^*_{1238}(p\pi^-)p\pi^+\pi^0$	0.01±0.01
G	$N^*_{1518}(p\pi^-\pi^0)p\pi^+$	0.11±0.04
H	$N^*1688(p\pi^-\pi^0)p\pi^+$	0.02±0.02
I	$N^*_{1518}(p\pi^+\pi^-)p\pi^0$	0.44±0.09
J	$N^*_{1688}(p\pi^+\pi^-)p\pi^0$	0.17±0.13
K	$pp\pi^+\rho_{763}(\pi^-\pi^0)$	0.07±0.07
L	$pp\pi^-\rho_{763}(\pi^+\pi^0)$	0.05±0.05
M	$pp\pi^0\rho_{763}(\pi^+\pi^-)$	~0
N	$pp\eta_{549}(\pi^+\pi^-\pi^0)$	0.02±0.01
O	$pp\omega_{782}(\pi^+\pi^-\pi^0)$	0.11±0.02
P	$pp\pi^+\pi^-\pi^0$	0.16±0.02

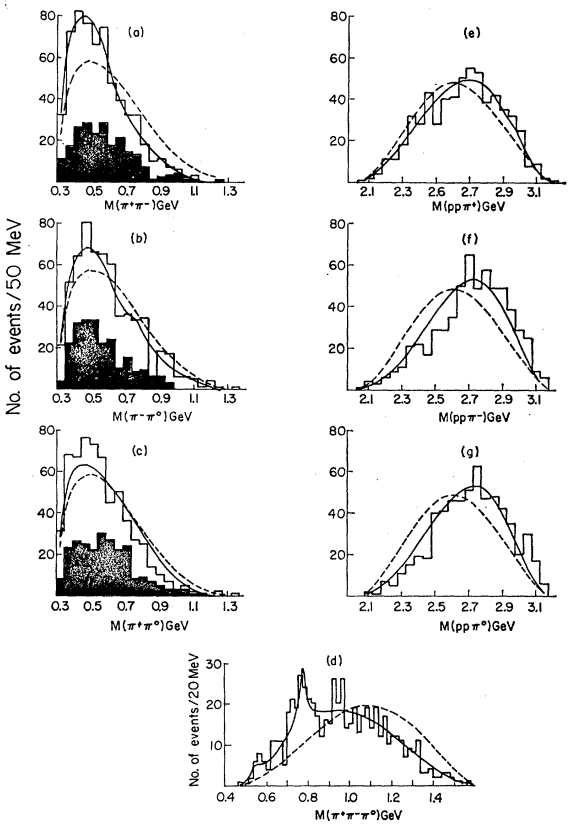

FIG. 26. Various invariant-mass distributions of $pp\pi^+\pi^-\pi^0$ final-state configurations. Shaded areas in (a), (b), and (c) include events with $M(p\pi^+)$ outside the $N^*_{1238}(p\pi^+)$ region.

IX. FOUR- AND FIVE-PION PRODUCTION REACTIONS

The c.m. angular distribution of the protons and pions in the final state $pp\pi^+\pi^+\pi^-\pi^-$ are shown in Figs. 27(a) and 27(b). The pions are isotropically emitted, while there is still some preference of the protons to be ejected in the forward-backward direction. There is no evidence for a peripheral production process in the final state. In general the various invariant-mass histograms follow their phase-space distribution. No attempt has been made to analyze this final state in terms of isobar production, because of the large number (as many as 56) of invariant-mass combinations which can be formed in this reaction. Four invariant-mass histograms which are of interest are given in Fig. 28 and are discussed in the next paragraphs.

A. The $p\pi^+\pi^+$ Combination

The invariant-mass histogram of the combination $p\pi^+\pi^+$ [Fig. 28(c)] has a peak above the phase-space curve (dashed line) at about $M=1570$ MeV. We have tried to explain this peak in terms of the well-established isobar channels (a) $pp\to N^*_{1238}(p\pi^+)p\pi^+\pi^-\pi^-$, (b) $pp\to N^*_{1238}(p\pi^+)N^*_{1238}(p\pi^+)\pi^-\pi^-$, (c) decay product of heavy isobars $pp\to N^*_{1920}(p\pi^+\pi^+\pi^-)p\pi^-$. Although some of these calculated mass distributions attain their maximum in the region of 1570 MeV, they cannot explain well the rather narrow peak of the data. The best fit to the data thus obtained was $(60\pm15)\%$ resonance at $M=1570$ MeV with a width of $\frac{1}{2}\Gamma=70$ MeV; $(25\pm15)\%$ phase space; and $(15\pm15)\%$ single $N^*_{1238}\pi^+$ mass distribution. It is worth noting that the invariant-mass histogram $M(p\pi^+)$ is consistent with the same channel mixture that was needed in the best fit to the $M(p\pi^+\pi^+)$ histogram.

B. The $\pi^+\pi^+\pi^-\pi^-$ Combination

There is no significant evidence for resonance structure in the $M(\pi^+\pi^+\pi^-\pi^-)$ histogram. However, because of the small total cross section of the $pp\pi^+\pi^+\pi^-\pi^-$ final state, one may use this histogram to estimate an upper limit to the reaction $pp\to ppf^*_{1250}(\pi^+\pi^+\pi^-\pi^-)$. From Fig. 28(d) it was estimated that $\sigma(pp\to ppf^*_{1250}(\pi^+\pi^+\pi^-\pi^-))<0.015$ mb.

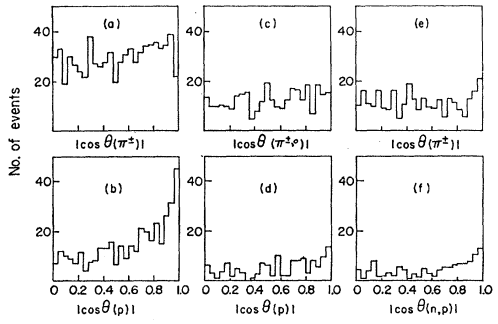

FIG. 27. Folded c.m. angular distributions of (a) $\pi^\pm$ and (b) $p_{1,2}$ in the $pp\pi^+\pi^+\pi^-\pi^-$ final state; (c) $\pi^{\pm0}$ and (d) $p_{1,2}$ in the $pp\pi^+\pi^+\pi^-\pi^-\pi^0$ final state; (e) $\pi^\pm$ and (f) n,p in the $np\pi^+\pi^+\pi^+\pi^-\pi^-$ final state.

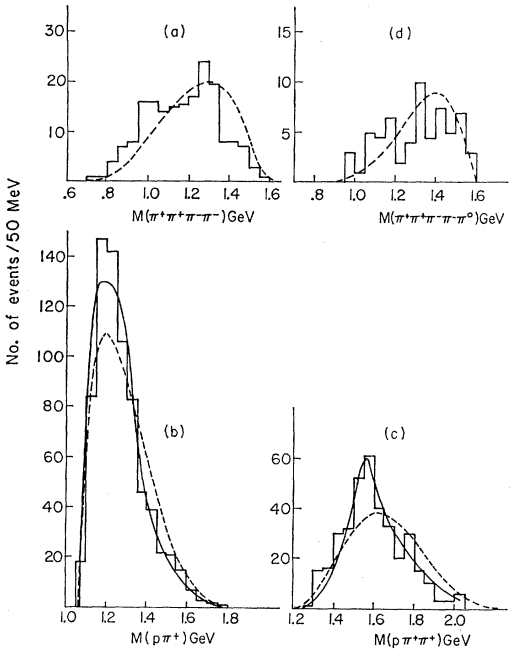

FIG. 28. Invariant-mass distributions of $pp\pi^+\pi^+\pi^-\pi^-$ final-state configurations (a) $\pi^+\pi^+\pi^-\pi^-$, (b) $p_{1,2}\pi^+$, (c) $p_{1,2}\pi^+\pi^+$, and (d) $\pi^+\pi^+\pi^-\pi^-\pi^0$ of the $pp\pi^+\pi^+\pi^-\pi^-\pi^0$ final state.

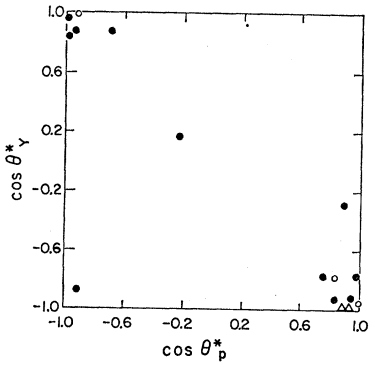

FIG. 29. Center-of-mass angular distributions of the two final-state baryons in the reactions $pp\to\Lambda pK^+$ and $pp\to\Sigma^0pK^+$. Filled circles correspond to Λ^0 events, open circles to Σ^0 events, and triangles to Λ-Σ^0 ambiguous events.

C. The $NN\pi\pi\pi\pi\pi\pi$ Final States

The c.m. angular distributions of both nucleons and pions in the final states $pp\pi^+\pi^+\pi^-\pi^-\pi^0$ and $np\pi^+\pi^+\pi^+\pi^-\pi^-$ are essentially isotropic [see, Figs. 27(c), 27(d), 27(e), and 27(f)]. As in the $pp\pi^+\pi^+\pi^-\pi^-$ final state, the different invariant-mass distributions are well described by phase-space distributions. Because of the large number of possible invariant-mass distributions that

TABLE VII. Partial cross sections for neutral strange-particle production in pp collisions at 5.5 GeV/c.

Final state	Events	$\sigma(\mu b)$	Partial sums (μb)	Reaction	Events	$\sigma(\mu b)$	Partial sums (μb)
ΛpK^+	13	35.8± 9.9		$\Lambda pK^+\pi^+\pi^-$	7	21.3± 8.1	
$\Sigma^0 pK^+$	4.5	16.0± 7.5		$\Lambda pK^0\pi^+\pi^0$	2	17.4±12.3	
$\Sigma^+ pK^0$	1	4.5± 4.5	56±13	$\Sigma^0 pK^+\pi^+\pi^-$	1	2.0± 2.0	
				$\Sigma^+ pK^0\pi^+\pi^-$	1	4.1± 4.1	45±15
$\Lambda nK^+\pi^+$	23	75.4±15.7					
$\Lambda pK^0\pi^+$	38.5	78.4±12.6		$\Lambda pK^0\pi^+\pi^+\pi^-$	0.5	0.9± 1.3	
$\Lambda pK^+\pi^0$	25.5	62.3±12.3	216±24	$\Lambda nK^+\pi^+\pi^+\pi^-$	0.5	1.1± 1.6	2±2
$\Sigma^0 pK^0\pi^+$	6.5	28.8±11.8		Missing mass			
$\Sigma^+ nK^0\pi^+$	1	4.1± 4.1					
$\Sigma^+ pK^0\pi^0$	2	9.4± 6.6	42±14	$\Lambda^0(\Sigma^0)$+2 prongs	7.5	30.5±11.5	
				K^0+2 prongs	6.5	28.2±11.0	59±16
npK^0K^+	3.5	19.4±10.4					
ppK^0K^0	2.5	6.4± 4.0	26±11	Unfitted events	9	24.6± 8.3	25±8

Total cross section[a] for neutral-strange-particle production = 0.45±0.04 mb.

[a] A correction of 0.02 mb on the total cross section accounts for contamination and V^0 events decaying on the apex.

one may form, no attempt has been made to detect isobar production.

Some idea of the X^0 meson production in pp collisions can be obtained by studying the reaction $pp \to pp\pi^+\pi^-\pi^0\pi^+\pi^-$. About 20% of any X^0 mesons produced in the reaction $pp \to ppX^0$ will eventually decay into $X^0 \to \pi^-\pi^+\pi^0\pi^+\pi^-$ through the chain $X^0 \to \eta\pi^+\pi^-$ followed by $\eta \to \pi^+\pi^-\pi^0$. Study of the $M(\pi^+\pi^-\pi^0\pi^+\pi^-)$ histogram [Fig. 28(d)] shows three events in the X^0 mass region. Taking into account the decay rates of $X^0 \to \eta\pi\pi$ and $\eta \to \pi^+\pi^-\pi^0$,[12] one obtains an upper limit on the X^0 production cross section of $\sigma(pp \to ppX^0) < 11 \pm 5$ μb.

X. NEUTRAL-STRANGE-PARTICLE PRODUCTION

A. The $pp \to Y^0KN$ Reactions

A cross-section value of 52±13 μb was found for the ΛpK^+ and $\Sigma^0 pK^+$ final states, which amounts to about 12% of all neutral-strange-particle production in pp collisions at 5.5 GeV/c (see Table VII). The c.m. angular distribution of the two final-state baryons, given in Fig. 29, shows a marked forward-backward peaking. The Dalitz plot and the two-body invariant-mass histograms of the reaction $pp \to \Lambda pK^+$ are given in Figs. 30 and 31. An accumulation of events can be seen in the region of low $K\Lambda$ invariant mass. This accumulation may be attributed to the reaction

$$\text{(a)}\quad pp \to N^*_{1688}(\Lambda K^+)p$$

with an upper limit of 17±8 μb for the cross section.

B. The $pp \to \Lambda NK\pi$ Reaction

The cross-section value of the $pp \to \Lambda NK\pi$ reaction was found to be 216±24 μb, and consists of about 50% of all neutral-strange-particle production (see Table

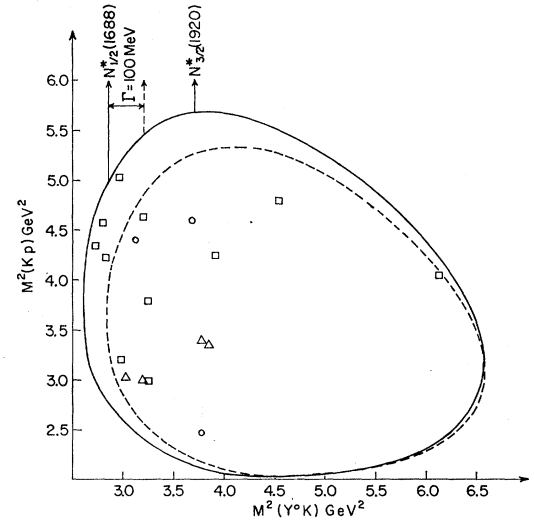

FIG. 30. Dalitz plot for $pp \to \Lambda pK^+$ (solid line and squares) and for $pp \to \Sigma^0 pK^+$ (dashed line and circles). Triangles describe two ambiguous events Σ^0-Λ (each event appears twice).

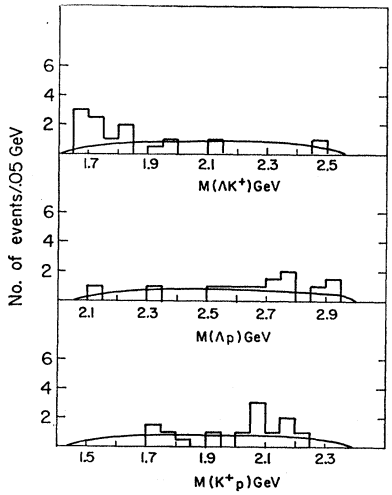

FIG. 31. Two-body invariant-mass distributions for $pp \to \Lambda pK^+$. Solid lines represent phase-space distributions.

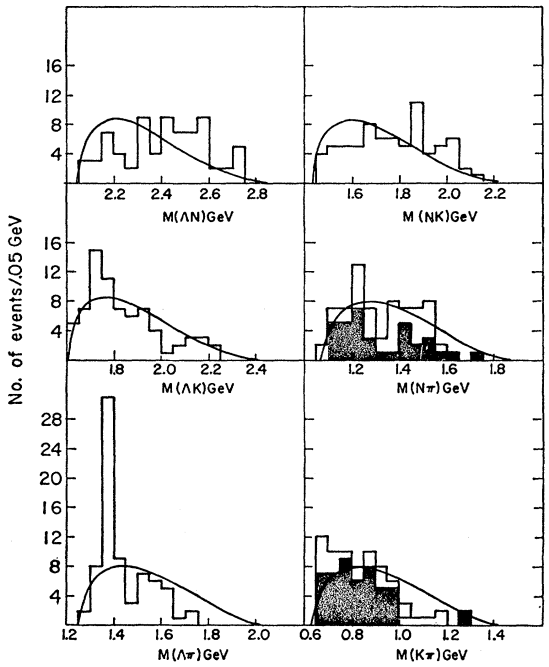

FIG. 32. Two-body invariant-mass distributions for $pp \to \Lambda NK\pi$. Events from reactions (b)–(d) are added together. The shaded areas describe events from reaction (b) in the $M(N\pi)$ histogram and events from reaction (b) and (c) in $M(K\pi)$ histogram.

VII). The three possible final states of this reaction are:

(b) $pp \to \Lambda^0 p K^0 \pi^+$,

(c) $\to \Lambda p K^+ \pi^0$,

(d) $\to \Lambda n K^+ \pi^+$.

Invariant-mass histograms of all possible two-body combinations are given in Fig. 32 together with their appropriate phase-space curves. In these histograms the events from reactions (b), (c), and (d) were added together, since no substantial differences were found among the various groups. Only in the $K\pi$ and $N\pi$ mass histograms are the distributions for certain charge configurations shown separately. The main features of these histograms are: (a) strong production of Y^*_{1385} resonance, (b) an enhancement in the ΛK invariant mass histogram at 1.7–1.8 GeV, (c) small, if any, production of N^*_{1238}, (d) no obvious deviation from phase space in the KN, ΛN, and $K\pi$ mass histograms. A cross section of 115 ± 15 μb was found for the reaction $pp \to Y^*_{1385} NK$ by fitting the $M(\Lambda\pi)$ histogram to a Y^*_{1385} Breit–Wigner curve and to phase-space curves.

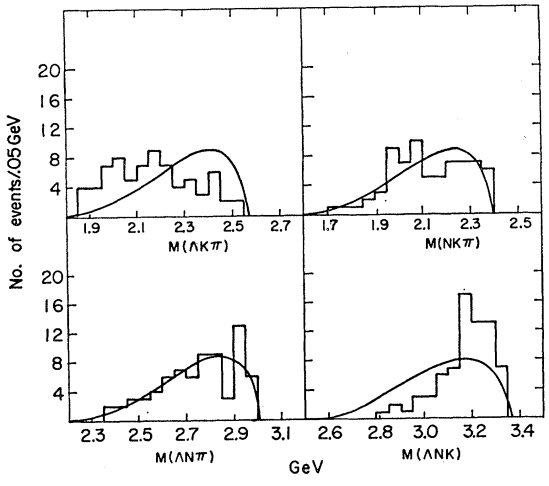

FIG. 33. Three-body invariant-mass distributions for $pp \to \Lambda NK\pi$. Solid lines represent phase-space distributions.

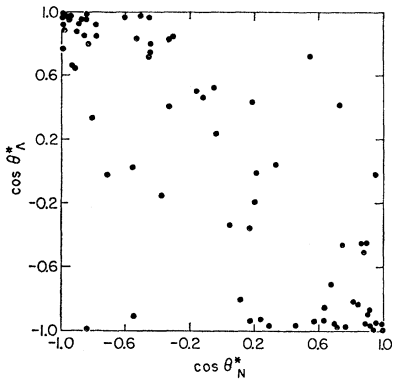

FIG. 34. Center-of-mass angular distribution of the two final-state baryons in $pp \to \Lambda NK\pi$ reaction.

In Figs. 33, 34, and 35 the three-body invariant-mass histograms and the c.m. angular distributions of the various particles are shown. There is an obvious forward-backward peaking in the angular distribution of the baryons, while the mesons are more isotropically distributed. The deviation from phase space in the ΛNK and ΛN mass histograms (Figs. 33 and 32) can be explained by the forward-backward peaking of the baryons.

In Fig. 36, are shown the ΛK and $\Lambda K\pi$ invariant-mass histograms in the Y^*_{1385} band $1.34 \leqslant M(\Lambda\pi) \leqslant 1.42$ GeV and outside this band. The possibility of attributing the accumulation of events around $M(\Lambda K\pi) \simeq 2$ GeV to

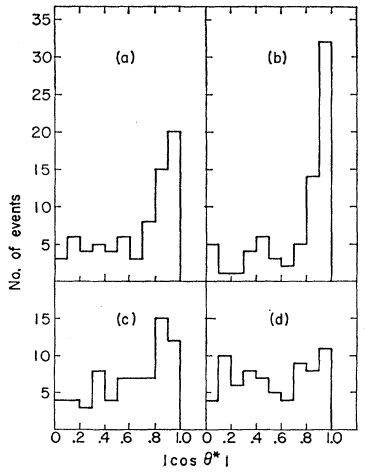

FIG. 35. Folded c.m. angular distributions of (a) Λ's, (b) nucleons, (c) kaons, and (d) pions.

the reaction

$$pp \rightarrow N^*_{1920}+N;\ N^*_{1920} \rightarrow Y^*_{1385}+K$$

was considered. As the mass sum of Y^*_{1385} and K is near 1920 MeV, it is expected that the accumulation of the events in the $M(\Lambda K\pi)$ plot, if indeed due to N^*_{1920} decay, will be shifted towards somewhat higher mass value. From isospin considerations, however, one expects

$$R=\frac{\sigma(pp \rightarrow N^{*++}+n)}{\sigma(pp \rightarrow N^{*+}+p)}=3$$

for an $I=\frac{3}{2}$ isobar. From the possible $Y^*_{1385}K$ decay in this experiment we obtain $R=0.2\pm0.1$, which is in contradiction with the assumption that the Y^*_{1385} is a decay product of N^*_{1920}. An alternative way to account for this accumulation of events is that the reaction $pp \rightarrow \Lambda NK\pi$ is dominated by the one-pion-exchange diagram shown in Fig. 37. The production of the Y^*_{1385} and K on the same vertex tends to enhance the low-invariant-mass region. This last explanation is also consistent with data on strange-particle production in π^--p interactions[26] where the final state $\Lambda K\pi$ is dominated by Y^*_{1385} production.

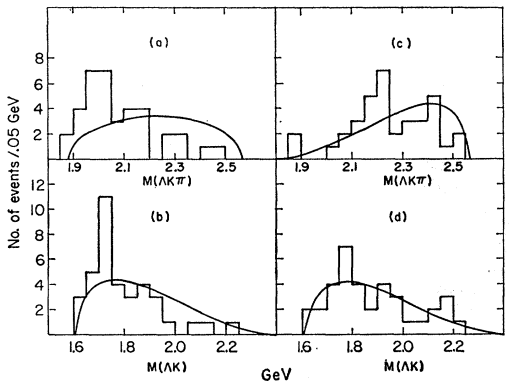

FIG. 36. $\Lambda K\pi$ and ΛK invariant-mass distributions for [(a) and (b)] Y^*_{1385} events, [(c) and (d)] non-Y^*_{1385} events, compared with appropriate phase-space distributions. The full line in (a) describes the $Y^*_{1385}K$ phase-space distribution in $pp \rightarrow Y^*NK$.

From Fig. 36 one can see that the enchancement in the $K\Lambda$ mass histogram at 1.7–1.8 GeV is mainly due to Y^*_{1385} production. This fact is also well demonstrated in the Dalitz plot where $M^2(\Lambda K)$ is plotted against $M^2(\Lambda\pi)$ for all events with $M(\Lambda K\pi)<2.05$ GeV (Fig. 38). In the same figure the Dalitz plot of the $\Lambda KN\pi$ final state is given for events with $M(\Lambda K\pi)$ in the 1.9–2.0-GeV region. Most of the events in this plot fall in the Y^*_{1385} region, and hence from kinematical constraints, the ΛK invariant mass attains a maximum in the 1.7–1.8-GeV region.

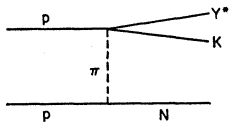

FIG. 37. One-pion-exchange diagram for the $pp \rightarrow Y^*_{1385}NK$ reaction.

XI. DISCUSSION AND CONCLUSIONS

In the present work a detailed analysis of all observable pp reaction final states has been carried out. Of the total pp cross section of 41.6 mb, we were able to account for about 32 mb. The rest of about 10 mb was mainly due to inelastic final-state events with more than one neutral particle. It was found that nucleons carry with them most of the momentum and are emitted in the forward-backward direction. The pions on the other hand, which are mainly decay product of isobars, are emitted much more isotropically and carry less momentum.

Isobar production is the most important phenomenon in pp collisions at 5.5 GeV/c. Six different isobars were identified, N^*_{1238}, N^*_{1420}, N^*_{1518}, N^*_{1688}, N^*_{1920}, and N^*_{2360}. The production of these isobars was sufficient to explain the various invariant-mass histograms. We are unable in this experiment to distinguish between isobars having nearby mass values—in particular, the recently reported possible isobars with $I=\frac{1}{2}$: N^*_{1700} and N^*_{1688},

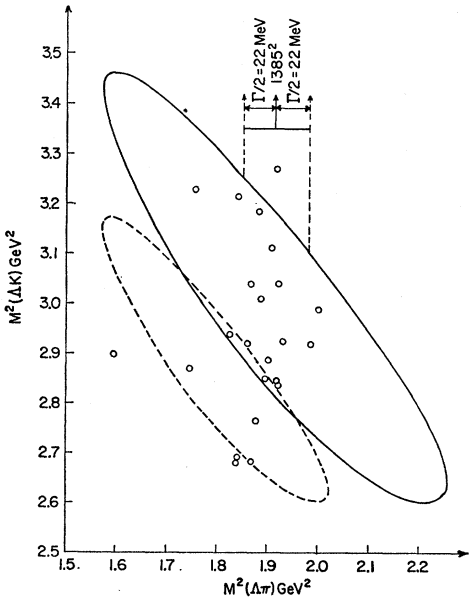

FIG. 38. Dalitz plot for $M^2(\Lambda K)$ versus $M^2(\Lambda\pi)$. The contours are for $M(\Lambda K\pi)=2$ GeV (full line) and 1.92 GeV (dashed line). The points represent $pp \rightarrow p\Lambda K\pi$ events with $M(K\Lambda\pi)<2.05$ GeV.

[26] D. H. Miller, G. Alexander, O. I. Dahl, L. Jacobs, G. R. Kalbfleisch, and G. A. Smith, Phys. Letters 5, 279 (1963) and references therein.

with spin and parity assignment $\frac{1}{2}^-$ and $\frac{5}{2}^-$.[27] No evidence for the production of the $I=\frac{3}{2}$ N^*_{1690} resonance is seen in the $M(p\pi^+)$ histogram of the reaction $pp \to np\pi^+$. The possible production of a $p\pi^+\pi^+$ resonance at 1580 MeV reported earlier[2] has been re-examined with three times as many statistics. While the peak observed in the $p\pi^+\pi^+$ combination in the final state $np\pi^+\pi^+\pi^-$ may be explained completely by the well-established resonances, it is unexplainable in the final state $pp\pi^+\pi^+\pi^-\pi^-$. However, because of the complexity of the $pp\pi^+\pi^+\pi^-\pi^-$ final state, no definite conclusion can be derived from the observed peak in the $p\pi^+\pi^+$ invariant-mass distribution.

There is very little evidence for the production of meson resonances. The total cross section for meson resonances is estimated as $\sigma(pp \to pp+\text{meson resonance}) < 0.13 \pm 0.03$ mb.

A large part of the iosbar cross section is connected with a quasi-two-particle final state amounting to 9.7 mb out of a 31 mb identified inelastic pp cross section. The various quasi-two-particle channels and estimates of their cross sections based on the assumptions stated in Sec. 4 are given in Tables III to VI. Two types of quasi-two-body reactions were observed:

(a) Single-isobar production, including $pp \to NN^*_{3/2}$ and $pp \to NN^*_{1/2}$ with total identified cross sections of 5.7 ± 0.2 mb and 3.2 ± 0.2 mb, respectively.

(b) Double isobar production, including $pp \to N^*_{1238}$ N^*_{1238} and $pp \to N^*_{1238}N^*_{1/2}$ with total identified cross section of 0.25 ± 0.04 mb and 0.51 ± 0.06 mb, respectively.

In strange-particle production, the most outstanding feature is the strong Y^*_{1385} production and the absence or very weak production of all other resonances. The enhancement in the $YK\pi$ invariant-mass distribution around 2 GeV for Y^*_{1385} events cound not be explained in terms of decay product of an $I=\frac{3}{2}$ isobar, as has been shown from isospin considerations. A production picture involving a one-pion-exchange mechanism in which the Y^*_{1385} and the K meson are produced on the same vertex could account for the copious Y^*_{1385} production and for the enhancement at low $M(Y^*_{1385}K)$ values.

Possible enhancements in the Λp system at threshold[28] and at 2.32 GeV,[29] which could be attributed to a $B=2$, $S=-1$ resonance, have been reported. In the present experiment, no significant enhancement in the ΛN invariant mass has been seen at these mass values (see Figs. 31 and 32).

For several isobars, decay branching ratios can be obtained from the cross section values given in Tables III to VI. The estimated branching ratios were used together with isospin and charge-symmetry relations to test the different channel cross-section values obtained in this work. No severe inconsistencies were found. However, because many cross-section values have a rather large error, we are quoting only the most reliable branching-ratio values.

(a) $\Gamma(N^*_{1518} \to n\pi^+)/\Gamma(N^*_{1518} \to p\pi^+\pi^-) = 0.77 \pm 0.45$ (see channel L in Table III and channel A in Table IV).

(b) $\Gamma(N^*_{1688} \to n\pi^+)/\Gamma(N^*_{1688} \to p\pi^+\pi^-) = 0.67 \pm 0.4$ (see channel N in Table III and channel B in Table IV).

(c) $\Gamma(N^*_{1688}(p\pi^+\pi^-) \to N^*_{1238}(p\pi^+)\pi^-)/\Gamma(N^*_{1688} \to p\pi^+\pi^-$ (all modes)$) = 0.74 \pm 0.14$ (see Sec. VI. 1), and

(d) $\Gamma(N^*_{1688} \to \Lambda K^+)/\Gamma(N^*_{1688} \to p\pi^+\pi^-) < 3.4\%$ (from Sec. X and channel B in Table IV).

The value (c) was estimated from the best fit to the $M(p\pi^+)$ with $M(p\pi^+\pi^-)$ in the N^*_{1688} band, which yielded 67% $N^*_{1238}(p\pi^+)$ and 33% phase-space distributions (see Sec. VI.1); and after proper correction to background events in the $M(p\pi^+\pi^-)$ distribution.

ACKNOWLEDGMENTS

We would like to thank CERN and the crew of the 81-cm hydrogen bubble chamber for enabling us to obtain the proton exposure. Our thanks are also due to the high-energy group of the University of Bern for letting us use their film share for the analysis of strange-particle production and six-prong events. Useful discussions with E. Gotsman are appreciated.

[27] See, for example, summary by Ch. Peyrou, in *Proceedings of the Oxford International Conference on Elementary Particles, 1965* (Rutherford High Energy Laboratory, Harwell, England, 1966), p. 131.

[28] A. C. Melissinos, N. W. Reay, J. T. Reed, T. Yamanouchi, E. Sacharidis, S. J. Lindenbaum, S. Ozaki, and L. C. L. Yuan, Phys. Rev. Letters **14**, 604 (1965).

[29] P. A. Piroue, Phys. Letters **11**, 164 (1964).